RHEOLOGICAL STUDY OF THE FORMATION OF A VISCOELASTIC FILM AT THE AIR-WATER INTERFACE IN L64 TRIBLOCK COPOLYMER AQUEOUS SOLUTIONS

by

William Diercxsens

A thesis submitted to the Faculty of the University of Delaware in partial fulfillment of the requirements for the degree of Master of Chemical Engineering

Spring 2015

© 2015 William Diercxsens
All Rights Reserved

ProQuest Number: 1596844

All rights reserved

INFORMATION TO ALL USERS
The quality of this reproduction is dependent upon the quality of the copy submitted.

In the unlikely event that the author did not send a complete manuscript
and there are missing pages, these will be noted. Also, if material had to be removed,
a note will indicate the deletion.

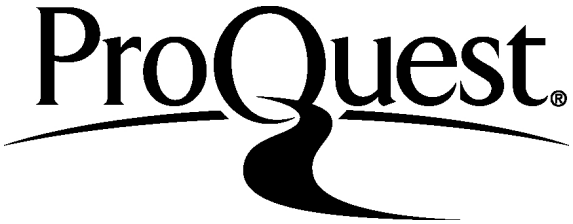

ProQuest 1596844

Published by ProQuest LLC (2015). Copyright of the Dissertation is held by the Author.

All rights reserved.
This work is protected against unauthorized copying under Title 17, United States Code
Microform Edition © ProQuest LLC.

ProQuest LLC.
789 East Eisenhower Parkway
P.O. Box 1346
Ann Arbor, MI 48106 - 1346

RHEOLOGICAL STUDY OF THE FORMATION OF A VISCOELASTIC FILM AT THE AIR-WATER INTERFACE IN L64 TRIBLOCK COPOLYMER AQUEOUS SOLUTIONS

by

William Diercxsens

Approved: _____
Yun Liu, Ph.D.
Professor in charge of thesis on behalf of the Advisory Committee

Approved: _____
Abraham M. Lenhoff, Ph.D.
Chair of the Department of Chemical and Biomolecular Engineering

Approved: _____
Babatunde A. Ogunnaike, Ph.D.
Dean of the College of Engineering

Approved: _____
James G. Richards, Ph.D.
Vice Provost for Graduate and Professional Education

ACKNOWLEDGMENTS

I am very grateful to have had the opportunity to participate in the Chemical Engineering dual degree program between the KU Leuven and the University of Delaware. I learned so much this year at the University of Delaware, especially while working in this prestigious research environment with a bunch of fantastic people in the Wagner and Liu research groups. Looking back the best choice I made in my studies was to participate in this program.

This thesis could not have been possible without the support and guidance of a lot of people. I would like to thank the people who made this exchange program with the University of Delaware possible: Professor Peter Van Puyvelde, Professor Paula Moldenaers, Professor Norman J. Wagner, Isabelle Benoit and Kathie Young. I especially would like to thank Professor Peter Van Puyvelde for believing in me, and giving me the opportunity to participate in this program.

I would like to thank my advisor professor Yun Liu and co-advisor professor Norman J. Wagner for offering me this thesis project and guiding me through my research and studies.

I would like to thank everyone in the Wagner and Liu research group for having me in their group and for all their help. I would like to specifically thank Simon Rogers and Doug Godfrin for their help with my thesis, and my office partners Jeff Richards and Jannat Nayem for being awesome office mates, and for the blissful coffee breaks.

Last but not least, I would like to thank my parents for all their support and help to make this exchange program in the USA possible.

TABLE OF CONTENTS

LIST OF TABLES vii
LIST OF FIGURES viii
NOMENCLATURE xii
ABSTRACT xv

Chapter

1 INTRODUCTION 1

2 BACKGROUND AND THESIS OUTLINE 3

2.1 Poly(ethylene oxide)-Poly(propylene oxide)-Poly(ethylene oxide) Block Copolymers 3
2.2 Pluronic L64 3
2.3 Rheology: Oscillatory Shear Measurements 5

2.3.1 Basic concepts of rheology 5
2.3.2 Oscillatory shear measurements 6

2.4 SANS: Small Angle Neutron Scattering 9
2.5 Wilhelmy Plate Surface Tension Measurement 10
2.6 Thesis Outline 12

3 MATERIALS AND EXPERIMENTAL METHODS 13

3.1 Materials and Sample Preparation 13
3.2 Oscillatory Shear Measurements 13
3.3 SANS 14
3.4 Surface Tension Measurements 14

4 EXPERIMENTAL EVIDENCE OF THE FORMATION OF A FILM AT THE AIR-WATER INTERFACE 15

4.1 Oscillatory Shear Measurements 15
4.2 SANS 20
4.3 Surface Tension 22
4.4 Conclusion 23

5 EFFECT OF THE FILM FORMATION ON BULK OSCILLATORY SHEAR MEASUREMENTS 24

5.1 Interfacial Contribution: The Boussinesq Number 24

5.2 Addition Model to Determine the Surface Moduli from the Apparent Bulk Moduli 25
5.3 Application of Addition Model on Cone and Plate Geometry 27
5.4 Conclusion 30

6 APPARENT 2D PHASE DIAGRAM 31

6.1 Apparent 2D Phase diagram 31
6.2 The Effect of the Kinetics on T.F1 and T.F2 35

6.2.1 Effect of kinetics 35
6.2.2 Kinetic study 39

6.2.2.1 Film region 1 40
6.2.2.2 Film region 2 46

6.3 Conclusion 48

7 EXAMINING THE PROPERTIES OF THE FILM 49

7.1 Strain Amplitude Sweep 49
7.2 Frequency Sweep 51
7.3 Conclusion 54

8 THE EFFECT OF INTERFACIAL FILMS ON BULK RHEOLOGY MEASUREMENTS 55

8.1 Oscillatory Shear Rheology Measurements 55
8.2 Steady Shear Rheology Measurements 56
8.3 Process to Detect the Interfacial Contribution 59
8.4 Conclusion 59

9 CONCLUSION AND FUTURE WORK 61

REFERENCES 63

LIST OF TABLES

Table 1: Parameters of the characteristic time model for 20wt% L64 in D_2O..... 44

LIST OF FIGURES

Figure 1: Schematic picture of the phase diagram of pluronic L64 in D_2O, replotted from *L. Lobry et al* [7]. The critical micelle concentration curve (CMC-CMT) and the cloud point curve (CPT) are determined by SLS (static light scattering) and turbidity measurements. The percolation temperature (P.T.) is measured by oscillatory shear measurements and is characterized by a sudden increase of the moduli at a certain temperature and composition. 4

Figure 2: Shear flow of a liquid between 2 plates separated by a distance d. The upper plate slides at a velocity V, and the bottom plate is fixed. 5

Figure 3: Illustration of an oscillatory rheology measurement on a cone and plate geometry with radius R and angle φ. 7

Figure 4: Illustration of strain (γ), shear rate ($\dot{\gamma}$) and stress (σ) as a function of time in a purely viscous (V), purely elastic (E) and viscoelastic (VE) material. 8

Figure 5: Illustration of the Wilhelmy plate method with width w, and thickness d. The perimeter length l = 2w+2d 11

Figure 6: Oscillatory shear measurement of a 25wt% L64-D_2O solution as a function of temperature on a cone and plate geometry with diameter d_c=40mm and angle φ=0.0195 rad. The temperature rate is 0.1ºC/min, ω=1.36 rad/s and γ_0=100%. 16

Figure 7: Oscillatory shear measurement of a 25wt% L64-D_2O solution as a function of temperature on a DIN couette geometry with bob diameter D_b=27.7mm, cup diameter D_c=30mm and bob length L_b=41.6mm. The temperature rate is 0.1ºC/min, ω=1.36 rad/s and γ_0=100%. 17

Figure 8: Oscillatory shear measurement of a 25wt% L64-D_2O solution as a function of temperature on a DIN couette geometry with bob diameter D_b=27.7mm, cup diameter D_c=30mm and bob length L_b=41.6mm. The temperature rate is 0.1ºC/min, ω=1.36 rad/s and γ_0=100%. The sample volume is reduced such that the geometry is sensitive to the air-water interface. 19

Figure 9: SANS results for a 20 wt% solution of L64 in D_2O at different temperatures. 21

Figure 10: Surface tension of a 20wt% solution of L64 in D_2O set at 43°C, measured with a Wilhelmy plate. The crosses show the actual temperature, and the circles represent the surface tension. 22

Figure 11: Oscillatory shear measurement of a 20wt% L64-D_2O solution as a function of temperature on a cone and plate geometry with diameter d_c=40mm and angle φ=0.0195 rad. The temperature rate is 0.1ºC/min, ω=1.36 rad/s and γ_0=1%. 28

Figure 12: Oscillatory shear measurement of a 20wt% L64-D_2O solution as a function of temperature on a DIN couette geometry with bob diameter D_b=27.7mm, cup diameter D_c=30mm and bob length L_b=41.6mm. The temperature rate is 0.1ºC/min, ω=1.36 rad/s and γ_0=1%. 28

Figure 13: Surface moduli of a 20wt% L64-D_2O solution as a function of temperature on a cone and plate geometry with diameter d_c=40mm and angle φ=0.0195 rad. The temperature rate is 0.1ºC/min, ω=1.36 rad/s and γ_0=1%. 29

Figure 14: Effect of the strain amplitude on oscillatory shear measurements on the cone and plate geometry with diameter d_c=40mm and angle φ=0.0195 rad. C=20wt% L64 in D_2O. The temperature rate is 0.1ºC/min, ω=1.36 rad/s. γ_0=100% and 1%. 32

Figure 15: Illustration of the film transition phases. The bottom graph shows the oscillatory shear measurement of a 25wt% L64-D_2O solution as a function of temperature on a cone and plate geometry with diameter d_c=40mm and angle φ=0.0195 rad. The temperature rate is 0.1ºC/min, ω=1.36 rad/s and γ_0=100%. 33

Figure 16: The apparent 2D phase diagram of L64 in D_2O. The CMC-CMT and the cloud point temperature (CL.T.) from the bulk phase diagram are plotted as a reference. 34

Figure 17: The effect of the rate in oscillatory shear measurement of a 20wt% L64-D_2O solution as a function of temperature on a cone and plate geometry with diameter d_c=40mm and angle φ=0.0195 rad. ω=1.36 rad/s and γ_0=100%. 37

Figure 18: Oscillatory shear measurement of a 25wt% L64-D_2O solution as a function of temperature on a DIN couette geometry with bob diameter D_b=27.7mm, cup diameter D_c=30mm and bob length L_b=41.6mm. The temperature rate is 0.1ºC/min, ω=1.36 rad/s and γ_0=100%. The sample volume is reduced such that the geometry is sensitive to the air-water interface. The blue and yellow points are measured approximately 4 hours after the experiment. 38

Figure 19: Oscillatory shear measurement of a 20wt% L64-D_2O solution as a function of time at different temperatures on a cone and plate geometry with diameter d_c=40mm and angle φ=0.0195 rad. ω=1.36 rad/s and γ_0=1%. The surface loss moduli is not plotted, but follows the same trend as the surface storage moduli. 41

Figure 20: Rates of the film growth for both regions as defined in equation 25 and 26. 42

Figure 21: The characteristic time t_f as a function of temperature for a 20wt% L64-D_2O solution. 44

Figure 22: An illustrative estimation of the thermodynamic 2D phase diagram of L64 in D_2O. The CMC-CMT and the cloud point temperature (CL.T.) from the bulk phase diagram are plotted as a reference. 46

Figure 23: Oscillatory shear measurement of a 20wt% L64-D_2O solution as a function of time at different temperatures on a cone and plate geometry with diameter d_c=40mm and angle φ=0.0195 rad. ω=1.36 rad/s and γ_0=1%. The apparent loss moduli is not plotted, but follows the same trend. 47

Figure 24: The characteristic time t_f as a function of temperature for a 20wt% L64-D_2O solution. 48

Figure 25: Strain amplitude sweep on a cone and plate geometry (d_c=50mm, φ=0.0195 rad) for 20wt% L64 in D_2O at T=43ºC, and ω=1.36rad/s. 50

Figure 26: Strain amplitude sweep on a cone and plate geometry (d_c=40mm, φ=0.0195 rad) for 20wt% L64 in D_2O at T=55ºC, and ω=1.36rad/s. 50

Figure 27: Frequency sweep on a cone and plate geometry (d_c=50mm, φ=0.0195 rad) for 20wt% L64 in D_2O at T=40ºC, and γ_0=0.1%. 52

Figure 28: Frequency sweep on a Cone and Plate geometry (d_c=50mm, φ=0.0195 rad) for 20wt% L64 in D_2O at T=55ºC, and γ_0=1%. 52

Figure 29: Steady shear rheology measurements of 20 wt% L64 in D_2O at different temperatures on a cone and plate geometry with d_c=50mm and φ=0.0195rad (left) and on a DIN couette geometry with D_b=27.7mm, D_c=30mm and L_b=41.6mm (right). The equilibration time is 1 hour at 20 °C, 2 hours at 43°C and 40 mins at 55 °C. 10 points per decade are measured, and each point is averaged for 15 seconds with 15 seconds equilibration time. 57

NOMENCLATURE

A_S	Contact area between the geometry and the bulk phase
B_0	Boussinesq number [-]
CC	Concentric cylinder or couette geometry
CMC	Critical Micelle Concentration
CMT	Critical Micelle Temperature
C/P	Cone and Plate geometry
CPT	Cloud Point Temperature
D_b	Diameter of the bob in the couette geometry [mm]
d_c	Diameter of the cone in the cone and plate geometry [mm]
D_c	Diameter of the cup in the couette geometry [mm]
DWR	Double wall ring
E	Elastic
F	Force [N]
G^*	Complex modulus [Pa]
G'	Elastic or storage modulus [Pa]
$G"$	Loss modulus [Pa]
G'_a	Apparent storage modulus [Pa]
$G"_a$	Apparent loss modulus [Pa]
G'_s	Surface storage modulus [Pa.m]
$G"_s$	Surface loss modulus [Pa.m]
I	Scattering intensity [Counts.s^{-1}]
K	Stress constant [m^{-3}]

l	perimeter length of the Wilhelmy plate [m]
L_b	Length of the bob in the couette geometry [mm]
l_s	Characteristic length [-]
P_S	Perimeter in contact between the surface and the geometry
P.T.	Percolation Temperature
Q	Scattering vector [$Å^{-1}$]
R	Radius of the Cone [mm]
SANS	Small Angle Neutron Scattering
SDD	Sample-to-detector distance
t	Thickness of the interface [m]
t	time [s]
T	Temperature [°C]
T	Torque [F.m]
t_f	Characteristic time [min]
T.F1	Film region 1 transition temperature [°C]
T.F2	Film region 2 transition temperature [°C]
V	Viscous
VE	Viscoelastic
$\boldsymbol{\gamma}$	Surface tension [$N.m^{-1}$]
γ	Strain [%]
γ_0	Strain amplitude [%]
$\dot{\gamma}$	Shear rate [s^{-1}]
δ	Phase angle or loss angle [rad]
ε	energy transfer [-]

η	Dynamic shear viscosity [Pa.s]
λ	Wavelength [nm]
σ	Stress [Pa]
σ_S	Surface stress [Pa.m]
τ	Relaxation time [s]
φ	cone angle [rad]
ω	Angular frequency [rad.s^{-1}]

ABSTRACT

The formation of a film at the air-water interface in aqueous solutions of poly(ethylene oxide)-poly(propylene oxide)-poly(ethylene oxide) copolymers (commercially known as pluronics or poloxamers) and the effect this film can have have not been studied so far. This thesis provides a first comprehensive study of the film formed in aqueous solutions of pluronic L64, and provides a more general understanding of the formation of films at the air-water interface in solutions with surface active components.

Rheology measurements on different geometries and surface tension measurements provide evidence of the formation of a polymer film at the air-water interface in solutions of L64 in D_2O. Oscillatory shear measurements show a sudden increase in the apparent moduli at a certain temperature and composition which previous studies have attributed to a percolation phenomenon. Proof is provided that this increase in apparent moduli is due to the formation of a film at the interface, and not due to a percolation phenomenon. The surface effect is so big that the Boussinesq number in Cone and Plate geometries and even in Couette geometries is high enough to completely dominate the rheology measurements. A simple addition model is derived to determine the surface moduli from the apparent moduli measured in bulk rheology measurements. An apparent 2D phase diagram is determined in the concentration range of 5 to 25 wt% L64 in D_2O. Two distinct regions are observed: A high modulus film region 1 and a low modulus film region 2. Strain amplitude and frequency sweeps are used to characterize the microstructure of the film in both regions. Both regions show different properties with viscoelastic characteristics. Steady shear results show that high shear rates completely break down the structure in

film region 1, but don't affect the film in region 2. The kinetics of the formation of the film are investigated and show that the formation of the film is a slow kinetic process with nucleation properties that can take from 10 minutes to a couple hours depending on the temperature.

Interfacial effects can have a big effect on bulk rheology measurements that cannot be neglected, especially for surface active solutes. In oscillatory shear measurements they can lead to an overestimation of the moduli and in steady shear measurements they can lead to an apparent yield stress and an apparent shear thinning behavior. By using multiple geometries the interfacial contribution of rheology measurements can be detected and taken into account.

Chapter 1

INTRODUCTION

The migration of solute molecules to the air-water interface in aqueous systems is ubiquitous but still poorly understood. The solute molecules can form films at the interface that can greatly affect rheological measurements of the bulk properties [1]. Films at the air-water interface can also play an important role in the formation of undesirable protein aggregates [2], on the other hand films can also be used for interfacial synthesis [3].

Poly(ethylene oxide)-poly(propylene oxide)-poly(ethylene oxide) copolymers, commercially known as pluronics® (BASF) or poloxamers, are a class of nonionic macromolecular surfactants. Pluronics have very desirable amphiphilic properties that can easily be tuned by varying the chemical composition and temperature. This makes them attractive for a wide range of industrial applications such as detergency, dispersion stabilization, foaming, emulsification and inks [4]. Their ability to incorporate water insoluble particles as a nanocarrier is used in pharmaceuticals for drug solubilization and controlled release [5] [6]. The formation of a film at interfaces and the migration of the molecules in pluronic solutions to interfaces can have important consequences in its applications. For drug delivery purposes for example, the migration of pluronic molecules as nanocarriers to interfaces is absolutely important.

This thesis provides a first study and comprehensive investigation of the formation of a film in aqueous solutions of pluronic L64. The study of this system

provides better understanding of the formation of films at the interface, and can be used as a model to study interfacial effects in other systems.

Chapter 2

BACKGROUND AND THESIS OUTLINE

2.1 Poly(ethylene oxide)-Poly(propylene oxide)-Poly(ethylene oxide) Block Copolymers

Poly(ethylene oxide)-poly(propylene oxide)-poly(ethylene oxide) block copolymers, commercially known as pluronics® (BASF) or poloxamers, are a class of nonionic macromolecular surfactants. Pluronics are amphiphilic molecules that consist of a relatively hydrophobic PPO (poly(propylene oxide)) core block and two hydrophilic PEO (poly(ethylene oxide)) side-blocks. When dissolved in water micellar microstructures are formed that comprise of a hydrophobic core and a diffuse hydrophilic corona region with substantial hydration [5]. The amphiphilic properties of pluronics depend on the PPO/PEO ratio, the molecular weight and the temperature [4]. The polarity of both PEO and PPO blocks decreases as the temperature increases [4]. This is why pluronics are more soluble at low temperatures. At low temperatures, the pluronics are present as unimers in solution. At the CMT (critical micelle temperature) the lower polarity of the PPO block drives the formation of micelles. At the CPT (cloud point temperature) the PEO blocks are dehydrated, and the copolymers phase separate from the water. Control of the PPO/PEO ratio and molecular weight gives pluronics the ability to tune the desired amphiphilic properties, leading to a wide range of industrial applications.

2.2 Pluronic L64

Pluronic L64 consists of 40wt% PEO and 60wt% PPO and has a total average MW of 2900. The notation ‘L’ indicates that the pluronic is in the liquid state at room

temperature [4]. A schematic picture of the phase diagram of pluronic L64 in D_2O, determined by *L. Lobry et al*. [7], is replotted in figure 1.

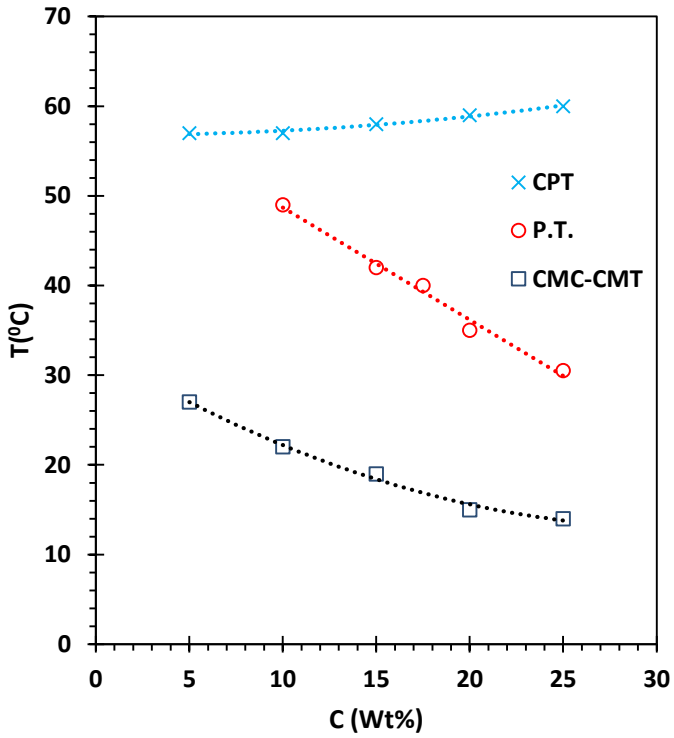

Figure 1: Schematic picture of the phase diagram of pluronic L64 in D_2O, replotted from *L. Lobry et al* [7]. The critical micelle concentration curve (CMC-CMT) and the cloud point curve (CPT) are determined by SLS (static light scattering) and turbidity measurements. The percolation temperature (P.T.) is measured by oscillatory shear measurements and is characterized by a sudden increase of the moduli at a certain temperature and composition.

At temperatures below the CMT, the copolymers are dissolved as unimers. Above the CMT, micelles are formed. The CMT decreases as the concentration of L64

increases, as is expected for pluronics [4]. At the CPT the copolymers phase separate from the solvent, and the solution becomes cloudy.

A sudden increase in the moduli at a certain temperature and composition has been shown to occur in the L64-D_2O system [7]. This sudden increase in the moduli has been reported to be a direct evidence of a percolation phenomenon in the L64-D_2O system [7]. This transition is shown as the P.T. line in figure 1. The problem with this conclusion is that a sudden increase in the moduli is not a requirement for a percolation phenomenon. Percolation could happen without significant changes in the moduli. As will be shown in chapter 4, this sudden increase in the moduli is in fact not due to a percolation phenomenon, but due to the formation of a film at the air-water interface.

2.3 Rheology: Oscillatory Shear Measurements

2.3.1 Basic concepts of rheology

Rheology studies the flow of matter, and the material response under applied stresses [8]. To illustrate the basic concepts, consider 2 parallel plates separated by a distance d with a liquid in between them, as shown in figure 2.

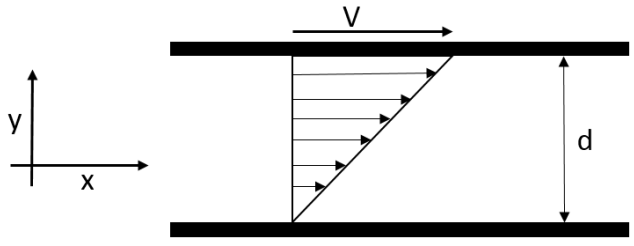

Figure 2: Shear flow of a liquid between 2 plates separated by a distance d. The upper plate slides at a velocity V, and the bottom plate is fixed.

By moving the top plate with a velocity V in the x direction while the bottom plate remains stationary, a velocity profile is induced in the liquid. Assuming the "no-slip" condition, the velocity gradient or shear rate $\dot{\gamma}$ is constant in the liquid [9]:

$$\frac{dv_x}{dy} = \frac{V}{d} = \dot{\gamma} = \text{constant} \quad (1)$$

To move the top plate with a velocity V in the x direction, a force F_{xy} or equivalently a stress σ_{xy} has to be applied. The dynamic shear viscosity (η) of the fluid relates the stress and the shear rate:

$$\sigma_{xy} = \eta\dot{\gamma} \quad (2)$$

The viscosity represents the resistance against flow [9]. For a Newtonian fluid the viscosity is constant and independent of the shear rate. For Non-Newtonian fluids, the viscosity will depend on the shear rate, as shear thinning or shear thickening can occur. Shear thinning means that the viscosity decreases with increasing shear rate, and shear thickening means that the viscosity increases with increasing shear rate.

2.3.2 Oscillatory shear measurements

Oscillatory rheology measurements are used to determine the properties of viscoelastic materials. Viscoelastic materials combine both viscous and elastic properties. In oscillatory rheology measurements, an oscillatory deformation is applied to the material, and the resulting oscillatory stress due to this deformation is measured. For the cone and plate geometry, the oscillatory deformation is applied to samples on the plate and the resulting torque (T) on the cone is measured and converted into a stress. This is illustrated in figure 3.

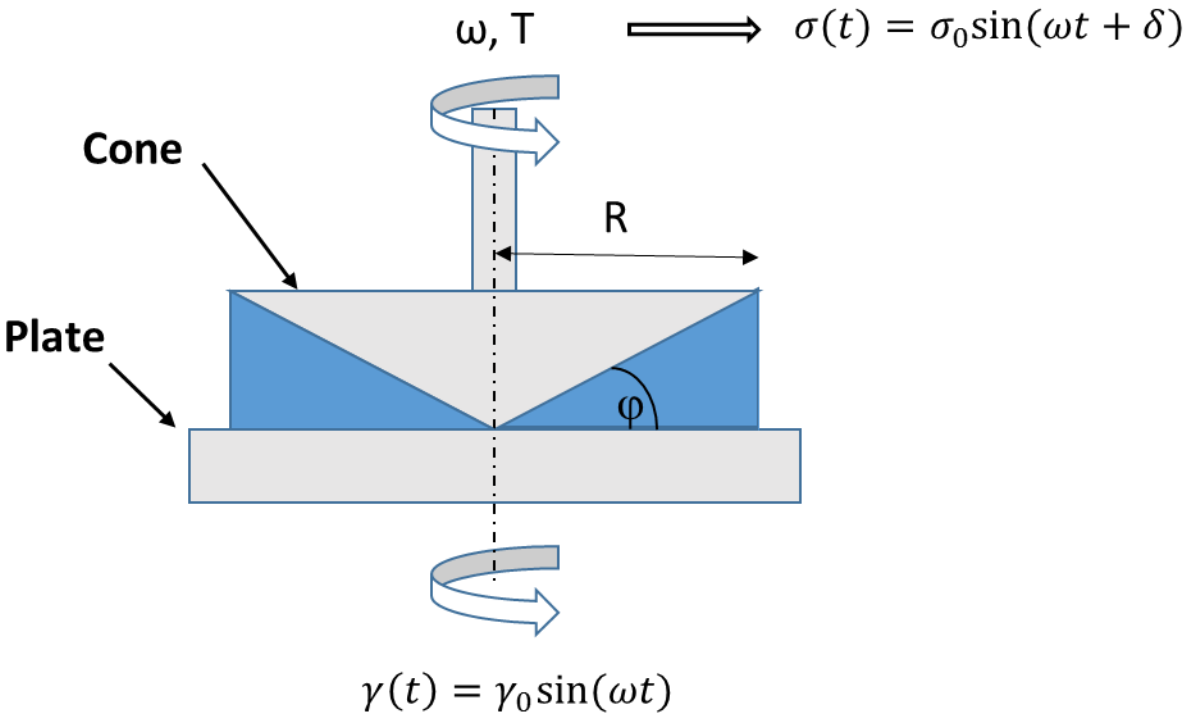

Figure 3: Illustration of an oscillatory rheology measurement on a cone and plate geometry with radius R and angle φ.

The sinusoidal deformation can be described by equation 3.

$$\gamma(t) = \gamma_0 \sin(\omega t) \quad 3$$

Where γ(t) (%) is the shear strain, γ_0 (%) is the strain amplitude, ω is the frequency and t is the time. The strain is defined as the ratio between the deformation and the distance between the plates. The strain in the example of figure 2 for a deformation of l in the x direction would be l/d. The resulting shear stress σ(t) can be described by equation 4.

$$\sigma(t) = \sigma_0 \sin(\omega t + \delta) \quad 4$$

Where σ_0 is the stress amplitude, and δ is the phase angle between the stress and the strain. The shear rate is the derivative of the shear strain with respect to time, and is given in equation 5.

$$\dot{\gamma}(t) = \gamma_0 \omega \cos(\omega t) = \gamma_0 \omega \sin(\omega t + 90°) \quad (5)$$

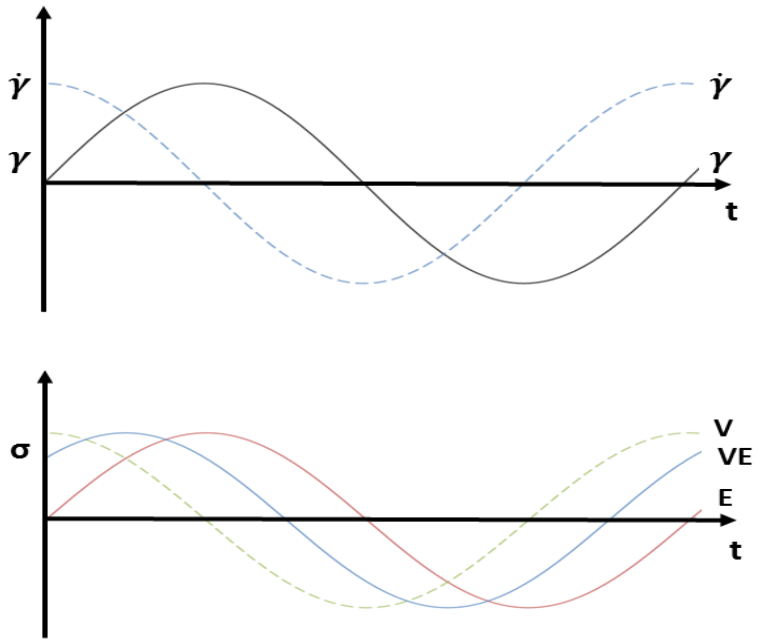

Figure 4: Illustration of strain (γ), shear rate ($\dot{\gamma}$) and stress (σ) as a function of time in a purely viscous (V), purely elastic (E) and viscoelastic (VE) material.

For a purely elastic material, the shear stress is in phase with the deformation or strain, and can be described by Hooke's Law, $\sigma_E = G' \gamma$, where G' is the elastic or storage modulus [9]. For a purely viscous material the stress obeys Newton's Law, $\sigma_V = \eta \dot{\gamma}$, where η is the viscosity of the material [9]. The resulting shear stress for a purely viscous material would be 90° out of phase with the strain. In a viscoelastic

material, the resulting stress is the sum of the elastic and viscous contribution and the phase angle is in between these two extremes, $0<\delta<90^{o}$ [9]. This is illustrated in figure 4 and described by equation 6 [9].

$$\sigma(t) = \sigma_E + \sigma_V = G'\gamma + \eta\dot{\gamma} = G'\gamma_0 \sin(\omega t) + \eta\gamma_0\omega \sin(\omega t + 90°) \quad (6)$$

$$\Leftrightarrow \quad \sigma(t) = (G' + iG')\gamma_0 = G^*\gamma_0$$

The complex modulus G^* is composed of an elastic contribution G′ and a viscous contribution G″. G′ is more commonly known as the storage modulus, and G″ as the loss modulus. The phase angle, more commonly known as the loss angle, relates the moduli by equation 7 [9].

$$\tan(\delta) = G''/G' \quad (7)$$

The moduli G′ and G″ are completely determined by σ_0 and δ, and are given by equations 8 and 9.

$$G' = \frac{\sigma_0}{\gamma_0} cos(\delta) \quad (8)$$

$$G'' = \frac{\sigma_0}{\gamma_0} sin(\delta) \quad (9)$$

2.4 SANS: Small Angle Neutron Scattering

Small angle neutron scattering is a measurement technique used to measure the structure of materials in the size scale of 1 to 500 nm [10]. Neutrons have no charge, so they are not affected by the electrons around the nucleus of an atom. Neutrons interact with atoms via short-range nuclear forces [11]. This gives neutrons the advantage of having a much longer penetration depth than charged particles, and

makes it possible to characterize structures in dense matter [11]. The wavelength of visual light ranges from 0.4 to 0.7 μm and this limits microscopes to visualize objects of micron sizes or bigger. Neutrons are also waves by the particle-wave duality, and thus they are characterized by a wavelength. The wavelength of neutrons is on the order of 10^{-10} m which makes it possible to use neutrons to measure length scales on the order of atomic sizes [11].

In neutron scattering experiments, a beam of neutrons is directed at a sample, and the intensity I of neutrons scattered is measured as a function of the scattering angle. The scattering angle is defined as 2θ. Usually the momentum transfer vector or scattering vector Q is used instead of the scattering angle. For elastic scattering the scattering vector Q is related to the scattering angle by the following equation [10].

$$Q = \frac{4\pi \sin(\theta)}{\lambda} \qquad 10$$

In 1954 Van Hove derived a general expression for I(Q,ε), the intensity I as a function of the scattering vector Q and the energy transfer ε. The result implies the following [10]:

> 'I(Q,ε) is simply the Fourier transform of a function that gives the probability of finding two atoms at a certain distance apart.'

This shows that the measured I(Q,ε) is related to length scales in a material, and thus neutron scattering can be used to determine the structure of materials.

2.5 Wilhelmy Plate Surface Tension Measurement

The Wilhelmy plate method is used to measure the interfacial tension. The method is illustrated in figure 5.

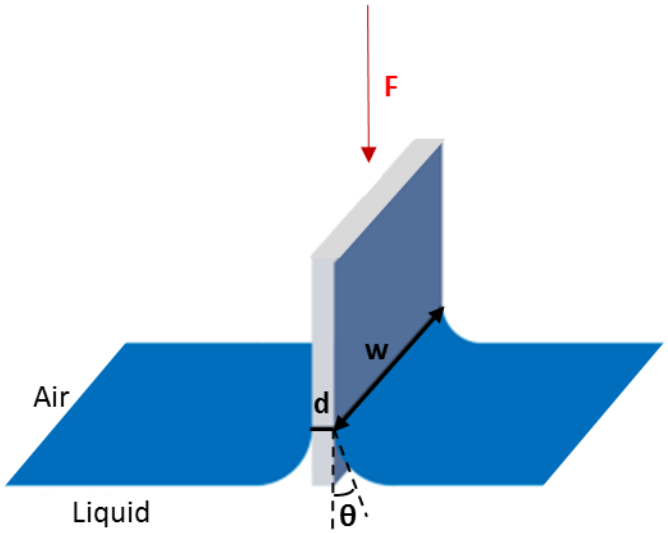

Figure 5: Illustration of the Wilhelmy plate method with width w, and thickness d. The perimeter length l = 2w+2d

In this method, the plate is lowered to the interface until it is wetted by the liquid. The plate is connected to a microbalance through a thin wire. The force acting on the plate due to the wetting of the plate is measured by the microbalance. This force is related to the interfacial tension, and this relationship is given by the following equation [12]:

$$\boldsymbol{\gamma} = \frac{F}{l * \cos(\theta)} \qquad 11$$

Where $\boldsymbol{\gamma}$ (N/m) is the interfacial tension, F (N) is the force measured by the microbalance, l (m) is the perimeter length of the plate and θ is the contact angle between the plate and the liquid.

The Wilhelmy plate method has the advantage that no correction for the measurement is necessary, because the weight of the film hanging on the plate is negligible [12]. Another advantage is that the plate can be placed at the interface, and does not require to be moved during the measurement. This allows the continuous determination of the surface tension in a wide range of timescales.

2.6 Thesis Outline

In chapter 3 the materials and experimental methods used for this thesis are specified. In chapter 4 evidence is provided of the formation of a film in the L64-D_2O system with results of rheology, SANS, and surface tension measurements. These results also prove that the increase of the apparent moduli in the L64-D_2O system is not due to a percolation phenomenon in the bulk as reported in literature [7], but that it is due to this phase transition at the air-water interface. The effect of the formation of this film on bulk oscillatory rheology measurements is discussed in chapter 5. A simple addition model is derived to separate the interfacial from the bulk contribution, and to determine the surface moduli of the film from the apparent moduli. In chapter 6 the 2D phase diagram of the film is determined, showing the occurrence of two distinct film regions in a certain temperature and composition range. The 2D surface rheological properties of both film regions are further investigated in chapter 7 with strain and frequency sweeps. The effect of the formation of films on the interpretation of rheological measurements, and a general method to detect the presence of an interfacial contribution is discussed in chapter 8. Finally chapter 9 includes the conclusion and suggestions for future work.

Chapter 3

MATERIALS AND EXPERIMENTAL METHODS

3.1 Materials and Sample Preparation

The pluronic L64 was obtained from BASF, and the deuterium oxide (D_2O) at 99.9% D was obtained from Cambridge Laboratories Inc. Both the L64 and the D_2O were stored at room temperature. The solutions were prepared by mixing the L64 in the D_2O at room temperature. The solutions were then stored in the fridge for a few days to ensure full dissolution, since pluronics are more soluble at lower temperatures. To ensure that all samples have the same history, the same procedure is used for all the samples.

3.2 Oscillatory Shear Measurements

The oscillatory shear measurements were performed with an ARES G2 strain controlled rheometer from TA Instruments. The following geometries were used:

- A stainless steel cone and plate geometry with a cone of 40mm diameter, and an angle of 0.0195 rad.
- A stainless steel cone and plate geometry with a cone of 50mm diameter, and an angle of 0.0195 rad.
- A concentric cylinder or couette geometry with a 27.7 mm diameter stainless steel DIN bob with a 41.6 mm length, and a 30 mm diameter aluminum cup.

The temperature was controlled accurately with a Peltier plate. A peltier solvent trap was used to minimize evaporation.

3.3 SANS

The SANS experiments were carried out on the NGB 30 m SANS instrument at the Center for Neutron Research (NCNR) at the National Institute of Standards and Technology in Gaithersburg, Maryland. Sample cells with Quartz windows of 1 mm thickness were used for all samples. The experiments were run in three different configurations:

- λ=6 Å, sample-to-detector distances (SDD) = 1.33 m for 300s.
- λ=6 Å, sample-to-detector distances (SDD) = 4 m for 600s.
- λ=6 Å, sample-to-detector distances (SDD) = 13.17 m for 900s.

Varying the SDD allows to probe a Q range of 0.004 to 0.45 $Å^{-1}$. An equilibration time of 10 minutes was applied between the different temperatures to ensure temperature equilibration.

To obtain the radially averaged corrected I(Q) results the raw data was reduced with standard data reduction procedure [13].

3.4 Surface Tension Measurements

The surface tension measurements were performed with a K10T tensiometer from Krüss, using a platinum Wilhelmy plate. The plate was cleaned by burning it with a propane torch.

Chapter 4

EXPERIMENTAL EVIDENCE OF THE FORMATION OF A FILM AT THE AIR-WATER INTERFACE

This chapter provides experimental evidence of the formation of a film at the air-water interface in aqueous solutions of pluronic L64. Oscillatory shear measurements, SANS and surface tension measurements are used to provide the evidence.

4.1 Oscillatory Shear Measurements

Figure 6 shows the results of oscillatory shear measurements of L64-D_2O solutions as a function of temperature measured with a cone and plate geometry. The moduli are named 'apparent moduli' G_a' and G_a'' because the bulk measurements are affected by the formation of a film at the air-water interface, as will be shown in this chapter.

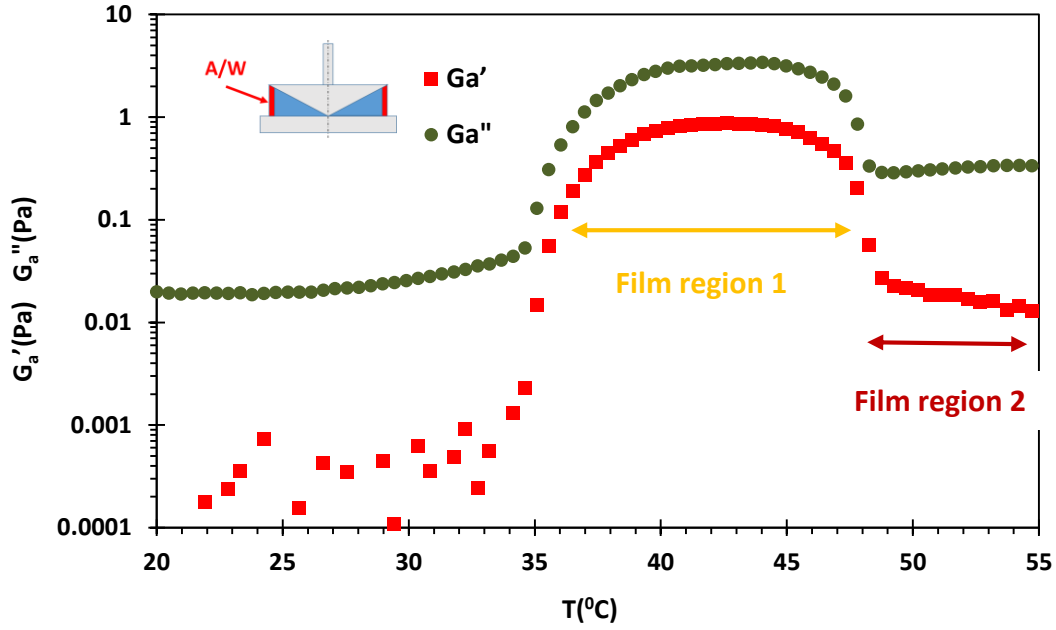

Figure 6: Oscillatory shear measurement of a 25wt% L64-D_2O solution as a function of temperature on a cone and plate geometry with diameter d_c=40mm and angle φ=0.0195 rad. The temperature rate is 0.1°C/min, ω=1.36 rad/s and γ_0=100%.

At temperatures below 35 °C the apparent storage modulus G_a' is smaller than the detection limit, and is very noisy, while the apparent loss modulus G_a'' is two orders of magnitude higher. This means that the solution is purely viscous at temperatures below 35 °C. At 36 °C, the apparent moduli G_a' and G_a'' suddenly increase 2 orders of magnitude and reach a plateau. The apparent moduli suddenly drop to a lower plateau at 48 °C.

Figure 7 shows the results of the same oscillatory shear measurements as a function of temperature on a couette geometry.

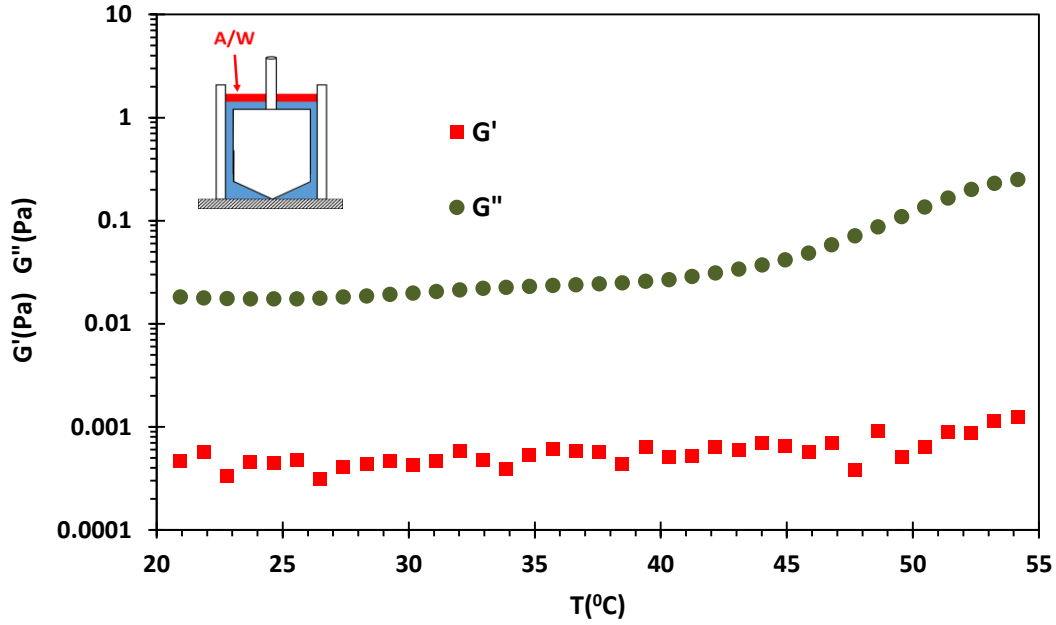

Figure 7: Oscillatory shear measurement of a 25wt% L64-D_2O solution as a function of temperature on a DIN couette geometry with bob diameter D_b=27.7mm, cup diameter D_c=30mm and bob length L_b=41.6mm. The temperature rate is 0.1°C/min, ω=1.36 rad/s and γ_0=100%.

This result shows no sudden jump in the moduli, and the solution remains almost purely viscous for all temperatures.

Couette and Cone and plate are two different geometries used to measure the rheological bulk properties, and should give the same results. In this case however the moduli show a completely different behavior for temperatures above 35 °C. The cone and plate geometry is sensitive to the interfacial rheological properties of the solution, while the current setup of the couette geometry is not. This is illustrated by the figures of the geometry in figures 6 and 7, where the air-water interface is highlighted. The measured moduli depend on the torque measured, which is directly proportional to the force and the distance. For the cone and plate geometry the torque measured has a

relatively higher contribution from the air-water interface, since it is located at the outer distance (R_c). In the current setup of the couette geometry the air-water interface is located above the cylinder where the gap between the cup and the bob is large. A large gap results in a lower stress on the bob, and an even lower torque measured since the distance is smaller. This makes this setup almost insensitive to the air-water interface.

These results indicate that the sudden jump in the moduli measured by the cone and plate geometry is due to its sensitivity to the air-water interface, and could be due to the formation of a film at the air-water interface.

Figure 8 shows the results of the same measurements on the same couette geometry, where the air-water interface has been lowered to the sensitive region of the couette as illustrated in the figure of the geometry in figure 8.

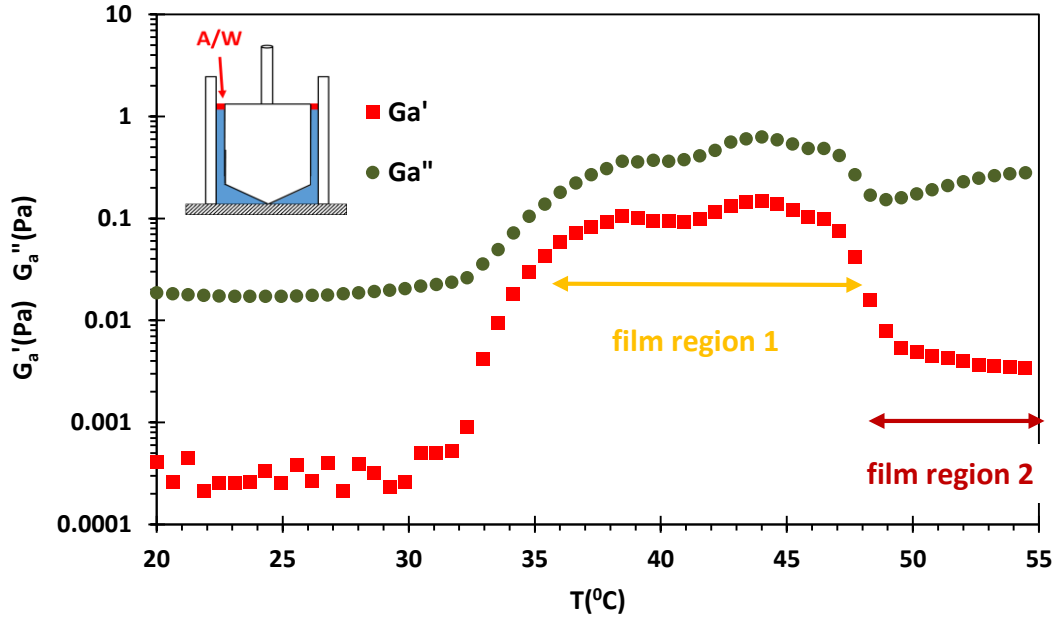

Figure 8: Oscillatory shear measurement of a 25wt% L64-D_2O solution as a function of temperature on a DIN couette geometry with bob diameter D_b=27.7mm, cup diameter D_c=30mm and bob length L_b=41.6mm. The temperature rate is 0.1ºC/min, ω=1.36 rad/s and γ_0=100%. The sample volume is reduced such that the geometry is sensitive to the air-water interface.

In this case the sudden jumps in the apparent moduli occurred, just like in the case of the cone and plate geometry. This is direct evidence that the sudden increase of the apparent moduli at a certain temperature and composition is not due to a percolation phenomenon, but due to the formation of a film at the air-water interface.

The temperature profile of the film shows two distinct regions: A high plateau region and a lower plateau region for temperatures above 48ºC. The high plateau region will be referred to as ‘film region 1’, and the lower plateau region as ‘film region 2’ as indicated in figure 6.

Since the measurements for the cone and plate geometry assume that the interfacial contribution is negligible, the measured moduli are in fact 'apparent moduli'. They are composed of an interfacial contribution and a bulk contribution and we find that the contribution to the G_a' is completely dominated by the surface film. This will be further discussed in chapter 5.

4.2 SANS

Small angle neutron scattering measurements are used to probe the bulk structure of materials. The I(Q) for a 20 wt% solution of L64 in D_2O as a function of temperature is shown in figure 9. The formation of micelles is characterized by the sudden increase of the intensity in the low Q-region and the emergence of a peak around 0.05 A^{-1}. In contrast with the oscillatory rheology measurements in figure 6, no sudden transition is observed in the SANS results. There is no obvious relation between the oscillatory rheology and the SANS results. This suggests that the transition measured in the oscillatory rheology measurements is not likely happening in the bulk, and thus is unlikely due to a bulk percolation phenomenon.

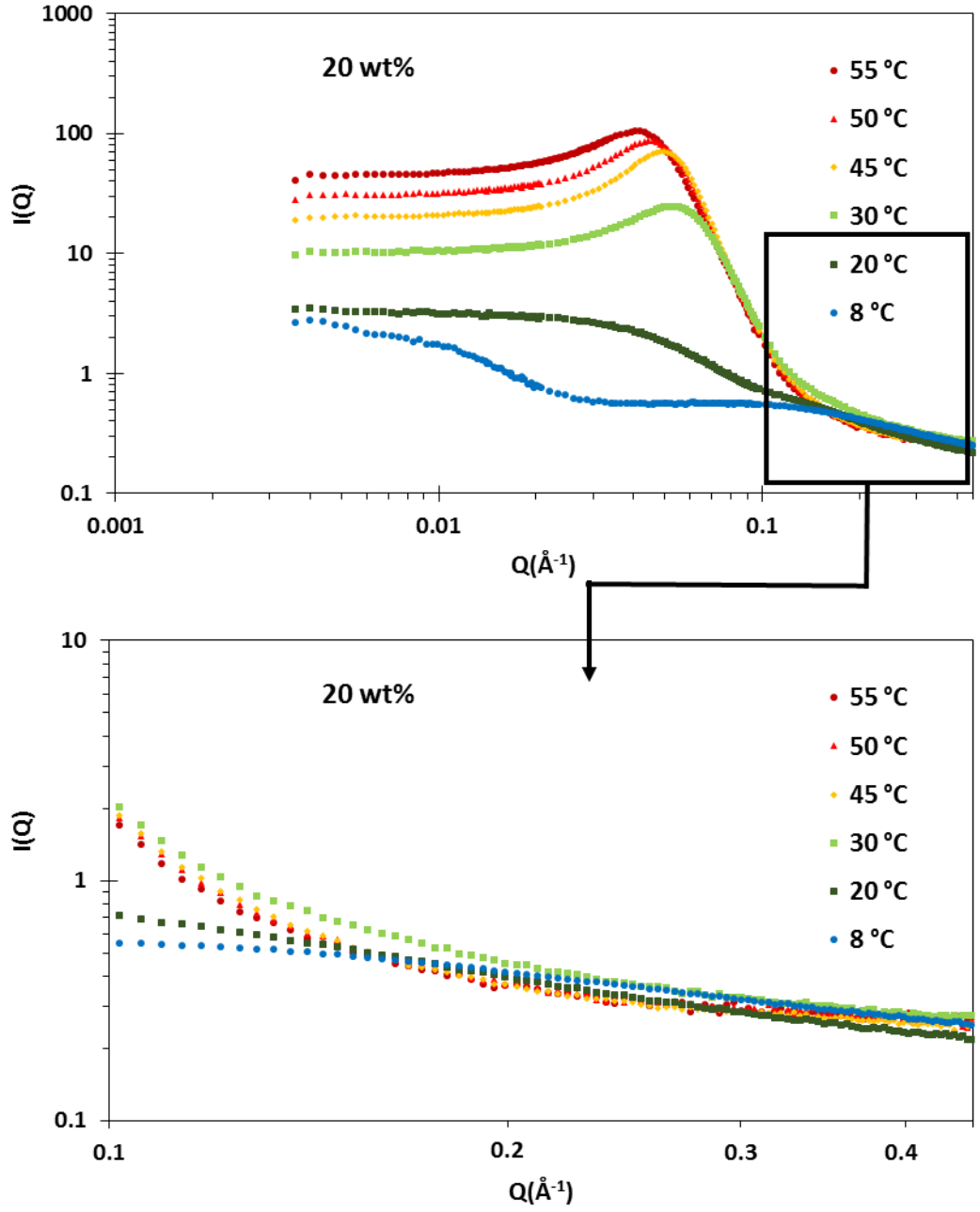

Figure 9: SANS results for a 20 wt% solution of L64 in D_2O at different temperatures.

4.3 Surface Tension

The existence of a viscoelastic film in the L64 – D_2O system at certain composition and temperatures, can also be shown with a direct interfacial measurement: Surface tension measurements.

The time dependent surface tension of a 20wt% solution of L64 in D_2O at 43 °C is shown in figure 10. To understand the data, it is important to remember how the measurement is performed. The Wilhelmy plate is wetted at the air-water interface, and the force acting on the plate is measured. This force is related to the surface tension. If however a viscoelastic film is formed at the air-water interface, the elastic properties of the film will have an effect on that force, and thus on the measured surface tension.

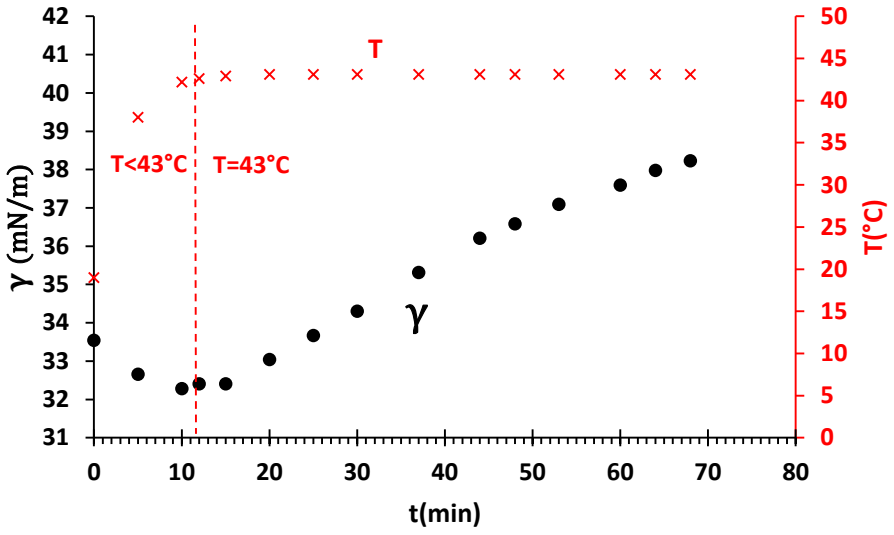

Figure 10: Surface tension of a 20wt% solution of L64 in D_2O set at 43°C, measured with a Wilhelmy plate. The crosses show the actual temperature, and the circles represent the surface tension.

As the temperature equilibrates to 43 °C, the surface tension decreases. After 15 minutes, the surface tension starts to increase. This increase in surface tension in time is due to the formation of a viscoelastic film at the air-water interface. Due to evaporation, the position of the interface lowers in time. As this happens, the viscoelastic film is moving down, and due to the film's elastic properties, the force on the plate increases.

4.4 Conclusion

A viscoelastic film at the air-water interface is formed in aqueous solutions of L64 in certain temperature regions. Oscillatory shear measurements on different geometries provide direct evidence that the sudden increase of the moduli at a certain temperature and composition is not due to a percolation phenomenon, but due to the formation of a film at the air-water interface. Surface tension measurements and bulk SANS measurements also support this conclusion. Two distinct regions are observed in the oscillatory shear measurements: A high plateau region that will be referred to as 'film region 1', and a lower plateau region that will be referred to as 'film region 2'.

Chapter 5

EFFECT OF THE FILM FORMATION ON BULK OSCILLATORY SHEAR MEASUREMENTS

The previous chapter provides evidence of the formation of a film at the air-water interface in aqueous L64 solutions. It also shows that this film greatly affects the bulk oscillatory shear measurements on a cone and plate geometry. In this chapter the effect of the film on the cone and plate measurements is examined in more details. The apparent moduli have contributions from both the film and the bulk. By removing the bulk contribution, the surface moduli of the film are determined.

5.1 Interfacial Contribution: The Boussinesq Number

Bulk rheology measurements are used to determine bulk properties of materials. With oscillatory shear measurements, the storage and loss modulus of materials are determined. Cone and plate, parallel plate and concentric cylinder or couette are examples of geometries used for bulk rheology measurements. These bulk measurements all assume that the relative contribution of the surface stresses to the bulk stresses are negligible. The surface contribution can be characterized by the Boussinesq number, which is a dimensionless number that relates the surface stresses to the bulk stresses [14]. It is defined as

$$B_o = \frac{\eta_S}{\eta_B l_s} \qquad 12$$

Where η_S is the surface viscosity, η_B is the bulk viscosity and l_S is a characteristic length scale that depends on the geometry used to measure the stresses. $l_S \approx A_B/P_S$ where P_S is the perimeter in contact between the surface and the

geometry and A_S is the contact area between the geometry and the bulk phase. In other words, in bulk rheology measurements the assumption is made that the Boussinesq number is so low that the contribution of the surface stress is negligible. When the surface viscosity becomes high enough, this assumption is not valid anymore. In this system the formation of a film at the air-water interface increases the surface viscosity, which increases the Boussinesq number, and as a consequence the bulk measurements are affected by the surface stresses. That is why the measured moduli are in fact apparent moduli G_a' and G_a''.

5.2 Addition Model to Determine the Surface Moduli from the Apparent Bulk Moduli

With the presence of a film at the air-water interface, the torque measured (T_m) by the rheometer can be modeled as the sum of the contribution of the bulk (T_b), and the contribution of the interface (T_{IF}):

$$T_m = T_b + T_{IF} \tag{13}$$

$$\Leftrightarrow$$

$$\frac{\sigma_m}{K} = \frac{\sigma_b}{K} + \frac{\sigma_{IF}}{K_{IF}} \tag{14}$$

Where in equation 14, K is the stress constant which is a geometry dependent constant that relates the measured torque to the stress (σ). Equations 15 to 18 give the expressions of the K constants for the bulk and the interface of the C/P and couette geometries.

$$K_{CP} = \frac{3}{2\pi R^3} \tag{15}$$

$$K_{CC} = \frac{(R_c^2 + R_b^2)}{4\pi L_b R_c^2 R_B^2} \quad (16)$$

$$K_{IF,CP} = \frac{1}{2\pi(R^2 t - Rt^2 + {}^{t^3}/_3)} \approx \frac{1}{2\pi R^2 t} \quad (17)$$

$$K_{IF,CC} = \frac{R_c^2 + R_b^2}{4\pi t R_c^2 R_b^2} \quad (18)$$

Where:

- R=radius of Cone
- R_c and R_b are the radius of the cub and bob respectively
- L_b = length of the bob
- t = thickness of the IF
- K_{cc} and K_{cp} are the stress constants for the concentric cylinder and cone and plate geometry respectively.
- $K_{IF,cc}$ and $K_{IF,cp}$ are the stress constants for the interface of a concentric cylinder and a cone and plate geometry respectively.

Replacing the stress constants in equation 14 results in expressions for the surface stress.

For the Cone and plate geometry:

$$t\sigma_{IF,CP} = \sigma_{S,CP} = (\sigma_m - \sigma_b)\frac{R}{3} = \sigma_{S,0}\sin(\omega t + \delta) \quad (19)$$

For the Concentric cylinder geometry:

$$t\sigma_{IF,CC} = \sigma_{S,CC} = (\sigma_m - \sigma_b)L_b = \sigma_{S,0}\sin(\omega t + \delta) \quad (20)$$

The bulk contribution (σ_b) can be approximately measured with a couette geometry that is insensitive to the interface. This insensitivity to the interface comes from the fact that P_S is small, so that the Boussinesq number is almost independent of the surface viscosity. These expressions can be used to remove the bulk contribution, and determine the rheological properties of the interface. The same equations from chapter 2 apply for the 2D rheological properties of the interface where the surface stress amplitude and the loss angle in equations 19 and 20 can be used to determine the surface moduli G'_s and G''_s.

5.3 Application of Addition Model on Cone and Plate Geometry

This model can now be applied to determine the surface moduli from the apparent moduli measured on the cone and plate geometry. The apparent moduli of a 20 wt% solution of L64 in D_2O for γ_0=1% as a function of temperature is shown in figure 11. To determine the surface moduli, the bulk contribution has to be removed as is shown in equation 19. The bulk contribution is determined by measuring the bulk moduli in a couette geometry which is insensitive to the interface. The bulk moduli measured are shown in figure 12. In this case the bulk contribution to the stress is negligible compared to the interfacial contribution when the film is formed. The bulk stress, or the corresponding bulk moduli will only measure noise at γ_0=1%. For temperatures above 48ºC the loss modulus does show an increase, but its value is still negligible compared to the apparent modulus at the same temperatures in the cone and plate geometry of figure 11.

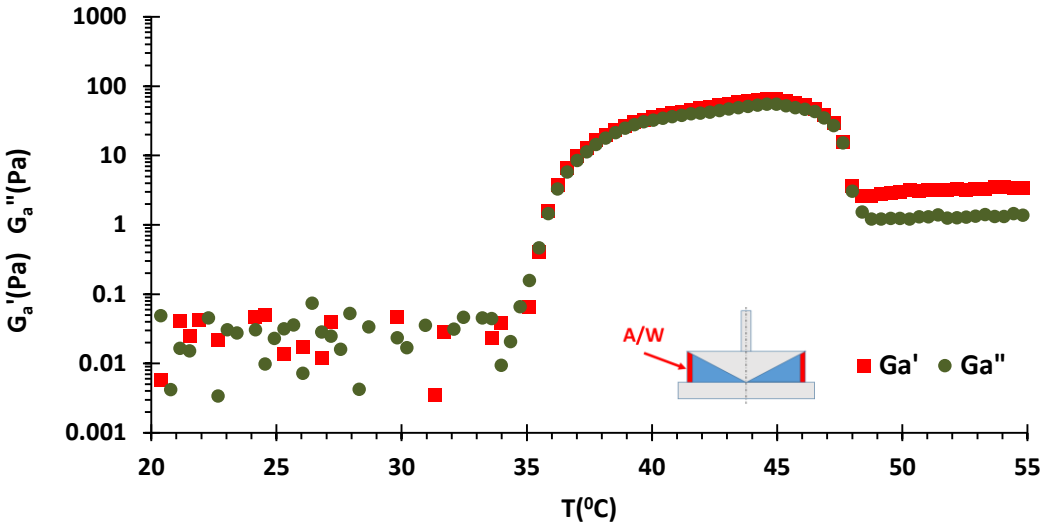

Figure 11: Oscillatory shear measurement of a 20wt% L64-D_2O solution as a function of temperature on a cone and plate geometry with diameter d_c=40mm and angle φ=0.0195 rad. The temperature rate is 0.1ºC/min, ω=1.36 rad/s and γ_0=1%.

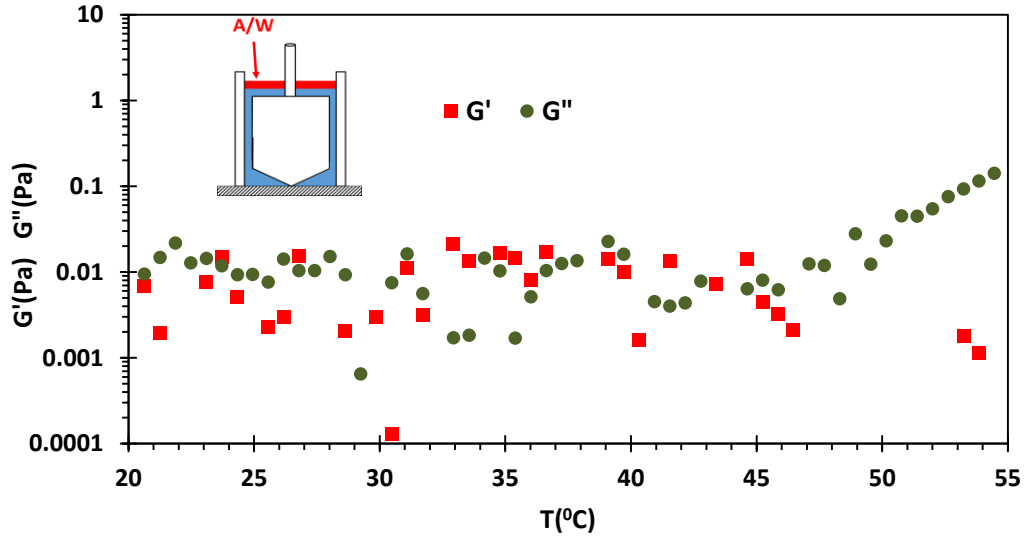

Figure 12: Oscillatory shear measurement of a 20wt% L64-D_2O solution as a function of temperature on a DIN couette geometry with bob diameter D_b=27.7mm, cup diameter D_c=30mm and bob length L_b=41.6mm. The temperature rate is 0.1ºC/min, ω=1.36 rad/s and γ_0=1%.

For negligible bulk contribution ($\sigma_b = 0$) the relation between the apparent moduli and the surface moduli in the cone and plate becomes simple:

$$G'_s = G'_a \frac{R}{3} \quad (21)$$

$$G''_s = G''_a \frac{R}{3} \quad (22)$$

This allows to calculate the surface moduli from the measured apparent moduli. The surface moduli of a 20 wt% L64 solution in D_2O as a function of temperature are shown in figure 13.

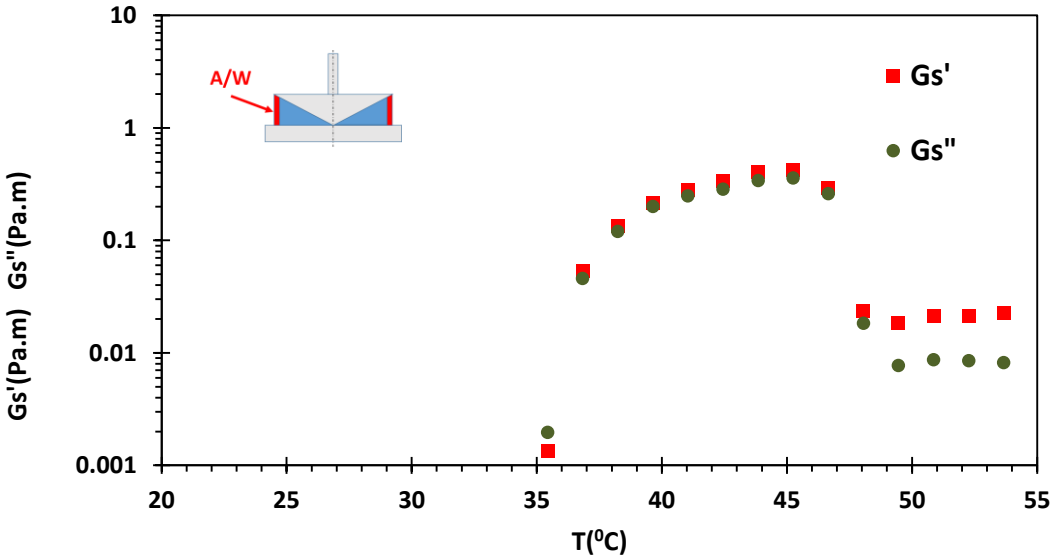

Figure 13: Surface moduli of a 20wt% L64-D_2O solution as a function of temperature on a cone and plate geometry with diameter d_c=40mm and angle φ=0.0195 rad. The temperature rate is 0.1°C/min, ω=1.36 rad/s and γ_0=1%.

5.4 Conclusion

The bulk rheology measurements are highly affected by the formation of a film at the air-water interface in the L64-D_2O system. With a simple additive model, the interfacial rheology can be determined from the apparent bulk rheology measurements. The surface moduli clearly show the formation of two distinct phases at the air-water interface: film region 1 and film region 2. In this case, the Boussinesq number for the cone and plate geometry is high enough to accurately measure the film properties.

Chapter 6

APPARENT 2D PHASE DIAGRAM

As shown in chapter 5, the rheological response of the film dominates over the bulk in the cone and plate geometry. In other words, the Boussinesq number is high enough for this system in the cone and plate geometry so that this geometry can be used to determine the 2D phase diagram.

6.1 Apparent 2D Phase diagram

An apparent 2D phase diagram can be constructed by varying the solution composition and the temperature. The temperature is increased at a slow rate of 0.1°C/min to ensure minimal lag of the sample temperature and to minimize the kinetic effects. The measurements are performed at a strain amplitude of 1 and 100%. A high strain of 100 % is used to be consistent with the literature set up [7]. As will be shown in chapter 7, these strain amplitudes are in the non-linear regime. Although the absolute values of the moduli depend on the strain amplitude in the non-linear regime the transition temperatures do not. At these strains the oscillatory shear measurements still qualitatively show the formation of the film regions at a certain temperature and concentration. A comparison of the oscillatory shear measurements for γ_0 of 1% and 100% in figure 14 shows that the strain amplitude does not affect the transition temperatures of the film. Therefore the transition temperatures can be determined with strain amplitudes in the non-linear regime. To characterize the properties of the microstructure of the film smaller strain amplitudes must be used in the linear regime, as will be shown in chapter 7.

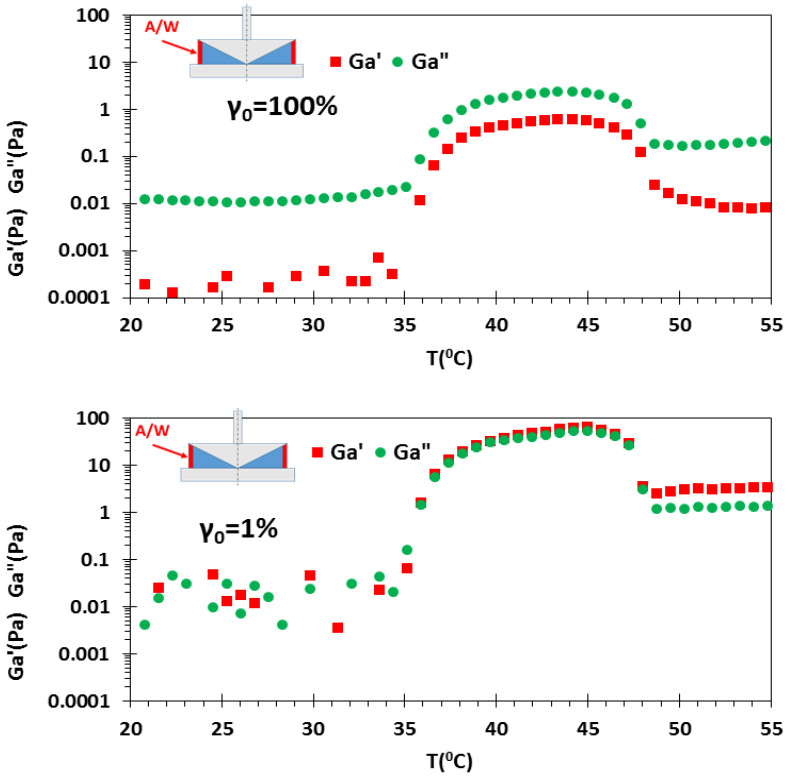

Figure 14: Effect of the strain amplitude on oscillatory shear measurements on the cone and plate geometry with diameter d_c=40mm and angle φ=0.0195 rad. C=20wt% L64 in D_2O. The temperature rate is 0.1ºC/min, ω=1.36 rad/s. γ_0=100% and 1%.

The temperature at which film region 1 is formed will be called 'T.F1'. The transition to film region 2 at higher temperatures will be called 'T.F2'.

The T.F1 is defined as the temperature at which the derivative of log(G″) with respect to temperature is at a maximum.

$$T.F1 = MAX\left(\frac{dlog(G'')}{dT}\right) \qquad 23$$

The T.F2 is defined as the temperature at which the derivative of log(G″) with respect to temperature is at a minimum.

$$T.F1 = MIN(\frac{dlog(G")}{dT}) \qquad 24$$

Both definitions of the transition temperatures are illustrated in figure 15.

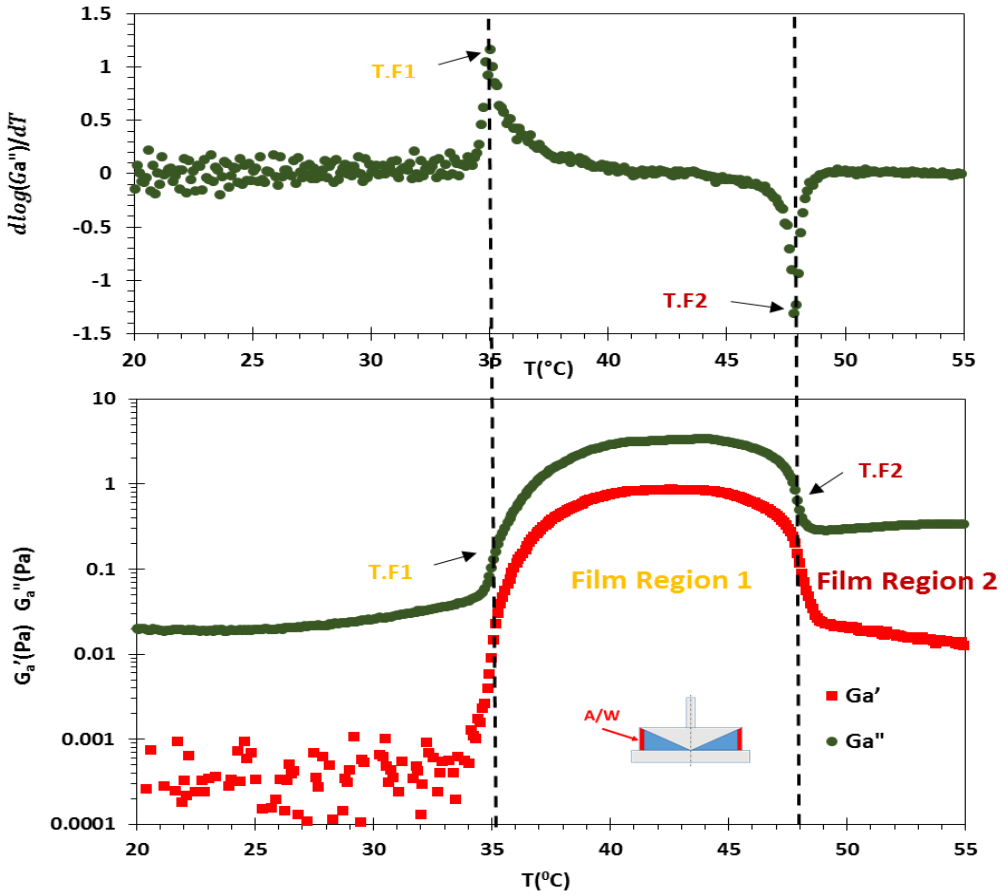

Figure 15: Illustration of the film transition phases. The bottom graph shows the oscillatory shear measurement of a 25wt% L64-D_2O solution as a function of temperature on a cone and plate geometry with diameter d_c=40mm and angle φ=0.0195 rad. The temperature rate is 0.1ºC/min, ω=1.36 rad/s and γ_0=100%.

By measuring the film transition temperatures for different concentrations at a rate of 0.1°C/min, the apparent 2D phase diagram is obtained in figure 16.

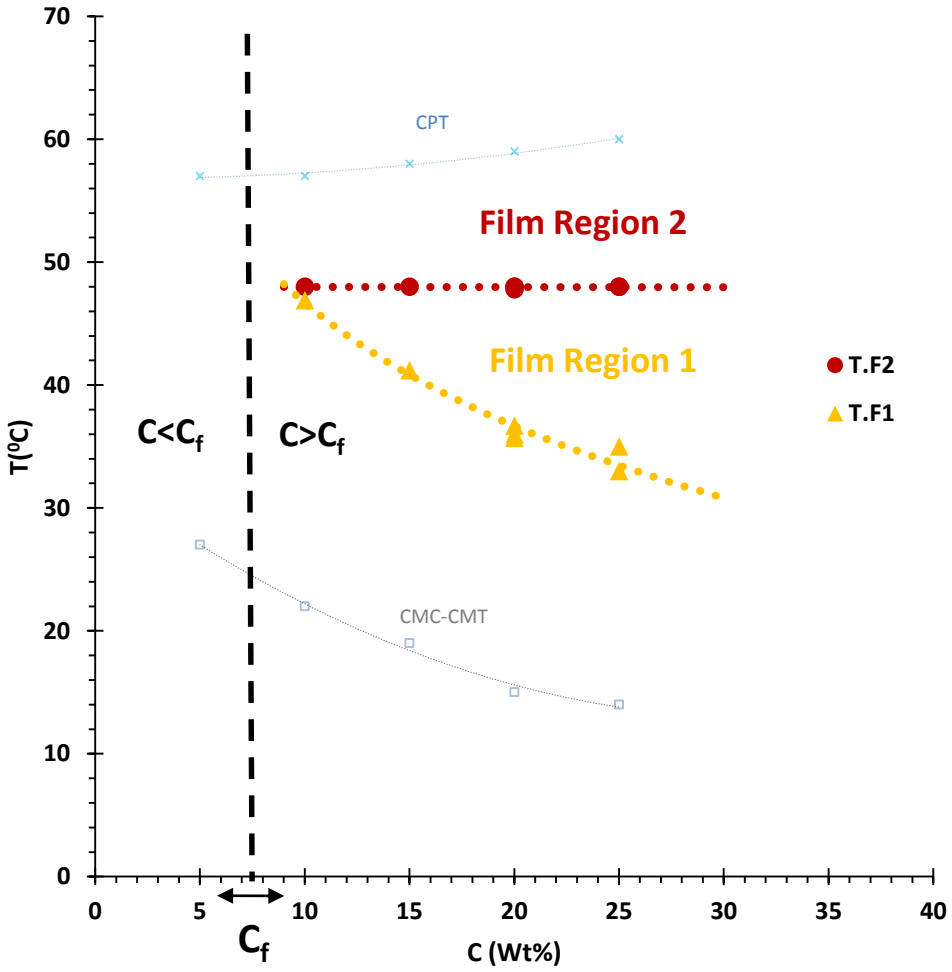

Figure 16: The apparent 2D phase diagram of L64 in D_2O. The CMC-CMT and the cloud point temperature (CL.T.) from the bulk phase diagram are plotted as a reference.

The T.F1 decreases as the concentration increases. The T.F2 does not depend on concentration, and is 48 °C for all the measured concentrations. For a concentration of 5 wt% L64, no apparent indication of the formation of a film in both region 1 and 2 is observed. This indicates that there is a critical concentration (C_f) between 5 and 10 wt% below which no film is formed.

6.2 The Effect of the Kinetics on T.F1 and T.F2

6.2.1 Effect of kinetics

When constructing the 2D phase diagram in figure 16, the assumption is made that a rate of 0.1 ºC/min is slow enough to avoid the effect of the kinetics. In other words, the hypothesis is made that thermodynamic equilibrium is reached fast enough so that at a rate of 0.1 ºC/min the film is constantly in thermodynamic equilibrium with the bulk. This hypothesis is tested by comparing temperature sweeps at different rates and by looking at the reversibility of the measurements.

The other issue to take into account for the temperature sweeps is the effect of solvent evaporation. The sample volume in the cone and plate geometry used is 0.34 ml. As the solvent evaporates faster than the solute, the concentration of the sample is affected. For slow temperature rates this effect is not negligible anymore, and the transitions may in fact be the transition temperatures corresponding to higher concentrations. The solvent trap used in the experiments helps minimize the effect of evaporation, but cannot completely eliminate it. By using geometries with higher sample volumes the concentration change due to solvent evaporation can be minimized.

The temperature sweeps at rates of 0.1, 0.5 and 2ºC/min in the cone and plate geometry show significant differences, as shown in figure 17. Faster temperature rates result in an increase of the T.F1 and lower the absolute values of apparent moduli in film region 1. At a rate of 2ºC/min there is no T.F1. This means that the film in film region 1 does not have enough time to form at this temperature rate. Clearly the formation of the film in region 1 is a very slow process, and the question arises as to whether or not a rate of 0.1 ºC/min is adequate to determine the equilibrium transition temperatures T.F1 and T.F2.

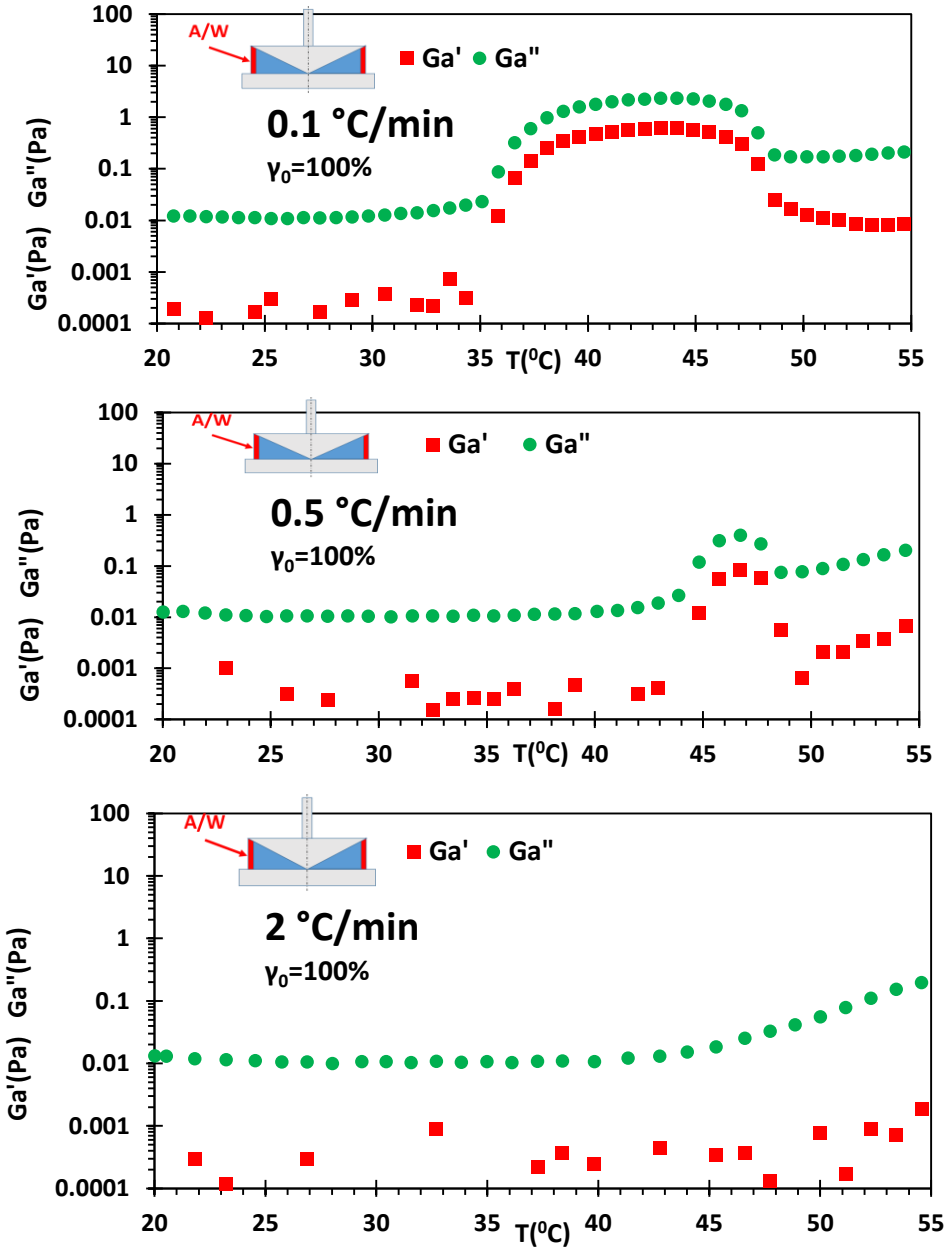

Figure 17: The effect of the rate in oscillatory shear measurement of a 20wt% L64-D_2O solution as a function of temperature on a cone and plate geometry with diameter d_c=40mm and angle φ=0.0195 rad. ω=1.36 rad/s and γ_0=100%.

A comparison of the heating and cooling temperature sweeps and its reversibility can give information about the kinetics of the formation of both film regions. The heating and cooling temperature sweeps of a 20 wt% solution measured in the couette geometry in the interface sensitive mode is shown in figure 18. Because of the high loading volume in a couette geometry, the concentration change due to evaporation of the solvent can be neglected. Hysteresis is observed, and this hysteresis cannot be attributed to evaporation effects.

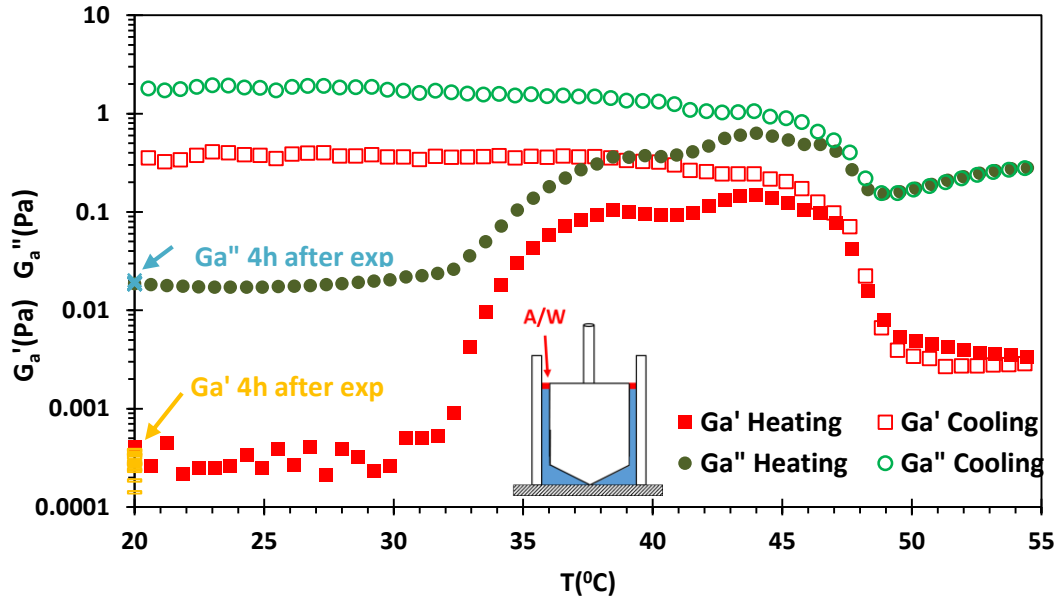

Figure 18: Oscillatory shear measurement of a 25wt% L64-D_2O solution as a function of temperature on a DIN couette geometry with bob diameter D_b=27.7mm, cup diameter D_c=30mm and bob length L_b=41.6mm. The temperature rate is 0.1°C/min, ω=1.36 rad/s and γ_0=100%. The sample volume is reduced such that the geometry is sensitive to the air-water interface. The blue and yellow points are measured approximately 4 hours after the experiment.

The T.F2 is independent of the rate used, and the transition is reversible. This shows that the T.F2 line in the 2D phase diagram is an equilibrium phase transition. For the T.F2, the hypothesis is valid.

The T.F1 line on the other hand is highly affected by the temperature rate, and the transition shows hysteresis. When cooling, the T.F1 transition does not occur at all, as can be seen in figure 18. When given enough time, T.F1 transition does occur as can be seen by the points measured 4 hours after the experiment. Clearly the formation and the dissolution of the film at the air-water interface is a slow process.

A comparison of the heating temperature sweep of a 25 wt% solution in the cone and plate geometry and the Couette geometry in figure 6 and 18 shows that the T.F1 transition is not affected by solvent evaporation effects at a rate of 0.1 ºC/min. If solvent evaporation was important, the T.F1 would be lower in the cone and plate geometry. However at a rate of 0.1 ºC/min thermodynamic equilibrium might not be reached fast enough. The hysteresis and rate dependence of the T.F1 transition suggest that the T.F1 line in the apparent 2D phase diagram is an overestimation, and that the thermodynamic T.F1 transition has to be shifted down towards lower temperatures.

6.2.2 Kinetic study

By studying the kinetics of the formation of the film in more detail, the time necessary for the film to form and the rate at which the response of the film grows can be quantified. Further study of the kinetic effects also allows to estimate the thermodynamic transition temperatures.

6.2.2.1 Film region 1

The characteristic time t_f is defined as the time necessary for the film to be detectable in the cone and plate geometry. This characteristic time depends on the temperature and the concentration. t_f is determined by measuring the moduli as a function of time at different temperatures as shown in figure 19. Once the film is formed, the film grows at a certain rate, depending on the concentration and temperature. This can be characterized by the rate of increase in surface moduli or equivalently the slope. For film region 1 the rate measured in a cone and plate geometry is defined as:

$$rate = \frac{10Pa - 1Pa}{t(G_a'' = 10Pa) - t(G_a'' = 1Pa)} R/3 \quad (25)$$

For film region 2 the rate is defined as:

$$rate = \frac{1.5Pa - 0.1Pa}{t(G_a'' = 1.5Pa) - t(G_a'' = 0.1Pa)} R/3 \quad (26)$$

Where the R/3 term comes from the conversion from apparent moduli to surface moduli as shown in equation 21 and 22.

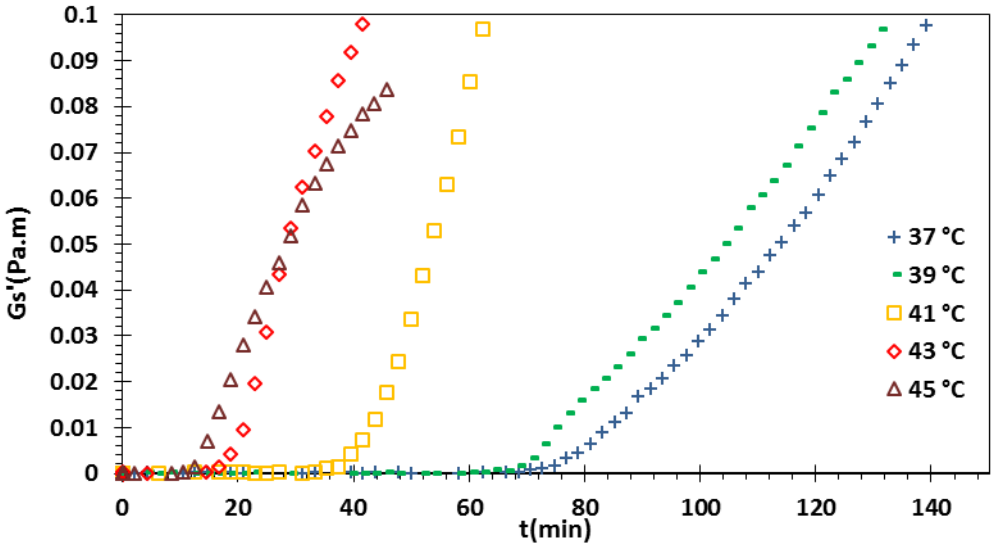

Figure 19: Oscillatory shear measurement of a 20wt% L64-D_2O solution as a function of time at different temperatures on a cone and plate geometry with diameter d_c=40mm and angle φ=0.0195 rad. ω=1.36 rad/s and γ_0=1%. The surface loss moduli is not plotted, but follows the same trend as the surface storage moduli.

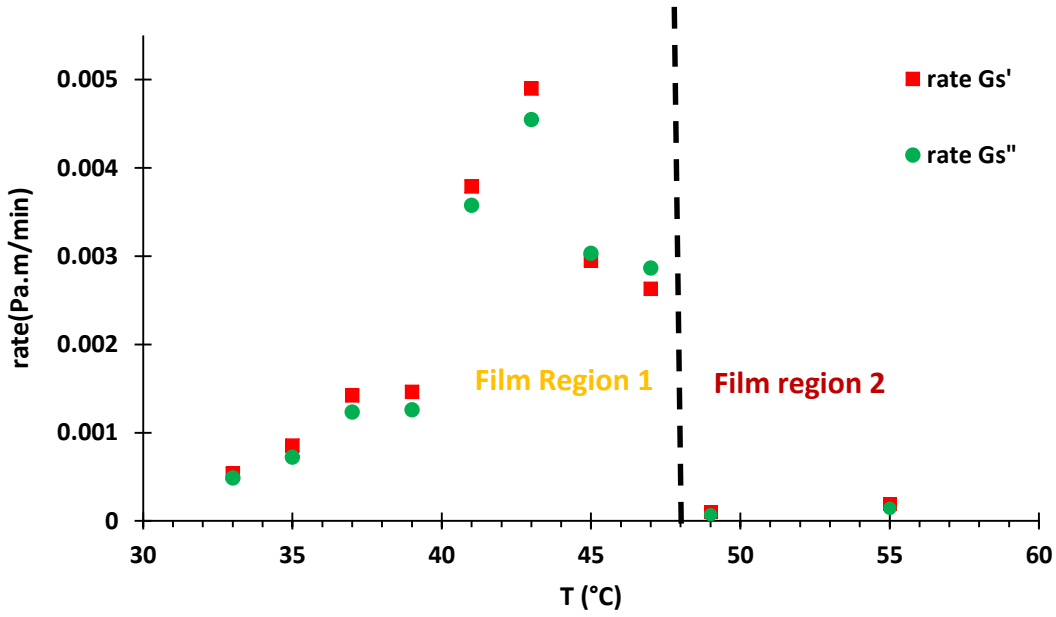

Figure 20: Rates of the film growth for both regions as defined in equation 25 and 26.

Before t_f the apparent moduli are noisy values around the detection limit of the instrument. The t_f can be defined as the time at which the surface storage modulus exceeds the detection limit of 0.00067 Pa (This corresponds to an apparent storage modulus of 0.1Pa in the C/P geometry with d_c=40mm). Once the film is formed, the surface storage modulus increases at a very high rate which implies that the film quickly grows or quickly becomes more resistant. This behavior shows a lot of analogy with a nucleation and growth process. An energy barrier has to be overcome to start the formation of the film. Once that energy barrier is overcome, the film grows fast. The higher the temperature, the faster that energy barrier can be overcome and the smaller the characteristic time.

It is possible that the film starts to form earlier than t_f and that it is just not detected before t_f. However since the moduli response increases so rapidly after t_f the actual characteristic time for formation of the film has to be very close.

The characteristic time for the film to form increases as temperature decreases as can be seen in figure 21. Interestingly this graph shows that it is possible to form the film at a temperature lower than the T.F1 line in the apparent 2D phase diagram of figure 16. This proves that at a rate of 0.1 °C/min the T.F1 line is overestimated, and that the formation of the film in region 1 happens at lower temperatures than the T.F1 line. Without kinetic effects, the T.F1 line would be shifted down towards lower temperatures. The characteristic time ranges from minutes at high temperatures to multiple hours at low temperatures. It is important to emphasize that the time necessary for the film to form is very long. At 33 °C for example, the characteristic time is more than 5 hours, which is way beyond the time routinely used for rheology measurements.

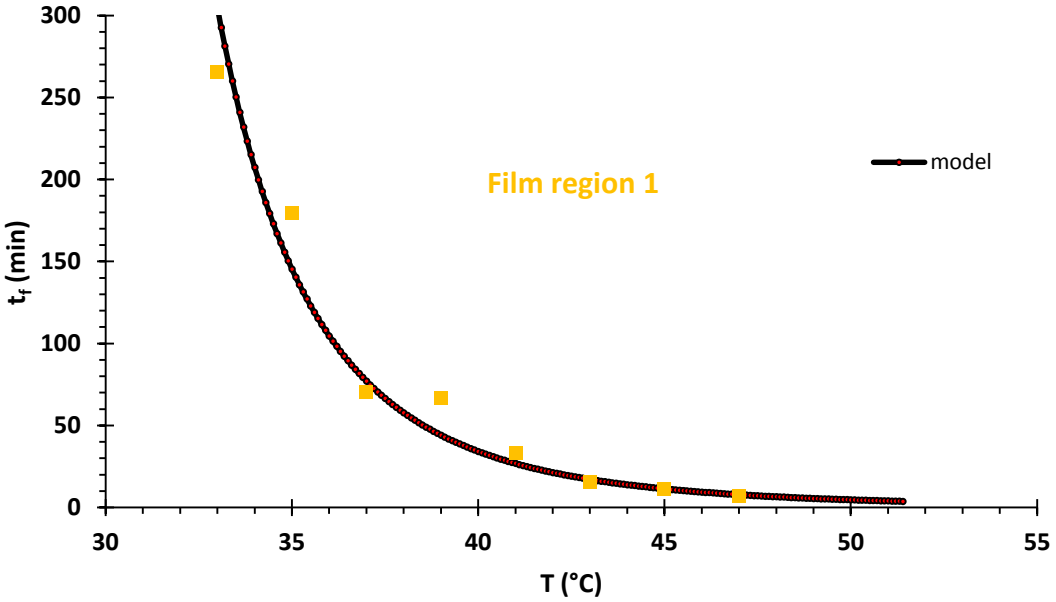

Figure 21: The characteristic time t_f as a function of temperature for a 20wt% L64-D_2O solution.

The following equation is used to model the characteristic time as a function of temperature:

$$t_f = A(T - T_0)^{-B} \qquad 27$$

Where A, B and T_0 are fitted parameter constants. The parameters found by fitting the results for the 20 wt% solution are shown in table 1.

Table 1: Parameters of the characteristic time model for 20wt% L64 in D_2O.

T_0	21.73 ºC
A	1.77 10^7 min/ ºC
B	4.53

This model predicts a vertical asymptote at $T=T_0$. This is the lowest temperature for which the film forms given an infinite amount of time. This physically corresponds to the thermodynamic transition temperature for film region 1. According to this model this transition temperature is 21.73 °C at a concentration of 20 wt%. If this procedure is followed for all the concentrations, an estimation of the thermodynamic 2D phase diagram can be obtained. An illustrative estimation of the thermodynamic 2D phase diagram is shown in figure 22. This illustrative thermodynamic 2D phase diagram is based on this model, and thus it is biased. Further study of different models at different concentrations is necessary to obtain a better unbiased estimation of the thermodynamic 2D phase diagram.

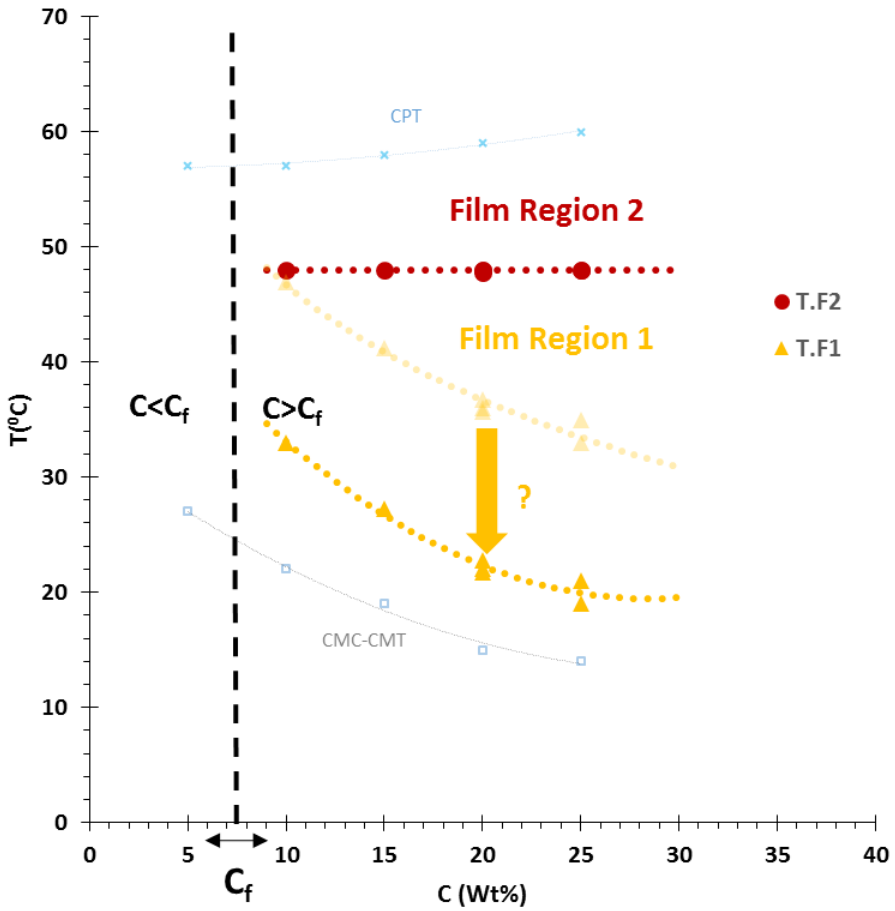

Figure 22: An illustrative estimation of the thermodynamic 2D phase diagram of L64 in D_2O. The CMC-CMT and the cloud point temperature (CL.T.) from the bulk phase diagram are plotted as a reference.

6.2.2.2 Film region 2

The same procedure can be followed for temperatures in film region 2. The samples are very quickly heated to the desired temperature in film region 2, such that the film in region 1 doesn't have time to form. The measurements of t_f are shown in figure 23 and summarized in figure 24. In region 2 the rates of increase in G' are much smaller than in region 1. The distinction between region 1 and 2 can also be made with

the characteristic time. When transitioning to temperatures in film region 2 the characteristic time jumps up, even though the temperature is higher in that region. This is in contrast with the T.F2 transition. The transition from film region 1 to film region 2 is immediate and reversible as seen in figure 18, but the complete formation of the film in region 2 is not immediate. This shows that the films in both regions are related, but they have different properties. The film in region 2 is a phase transition of film region 1.

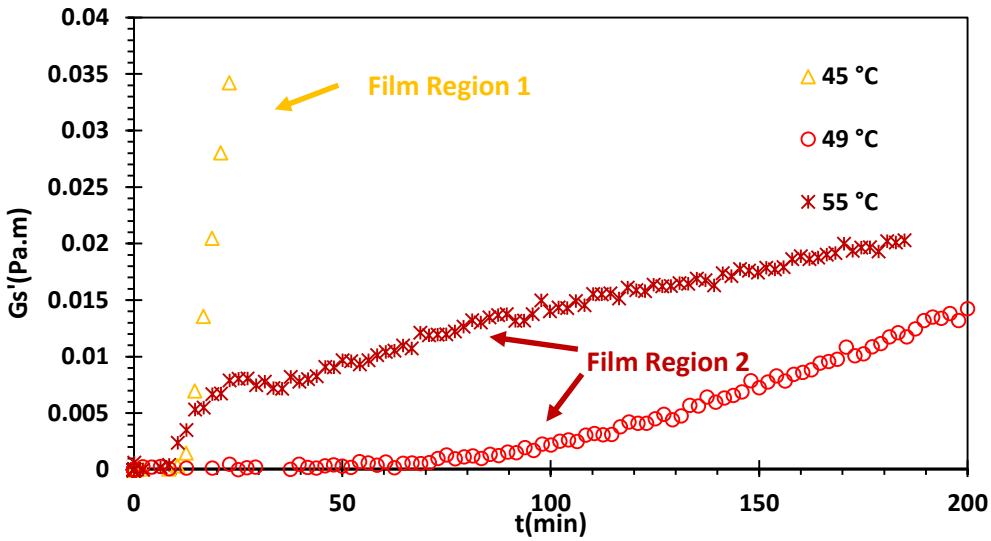

Figure 23: Oscillatory shear measurement of a 20wt% L64-D_2O solution as a function of time at different temperatures on a cone and plate geometry with diameter d_c=40mm and angle φ=0.0195 rad. ω=1.36 rad/s and γ_0=1%. The apparent loss moduli is not plotted, but follows the same trend.

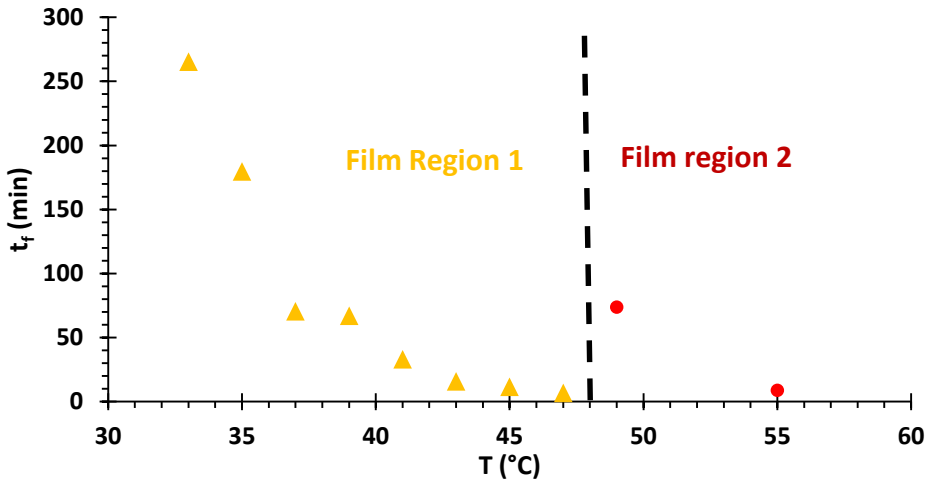

Figure 24: The characteristic time t_f as a function of temperature for a 20wt% L64-D_2O solution.

6.3 Conclusion

The formation of the film is a slow process driven by temperature and shows properties similar to a nucleation process. The slow kinetics of the formation of the film gives rise to an apparent 2D phase diagram, defined at a rate of 0.1 °C/min. results from the kinetic study show a clear distinction between the two film regions. The rate of increase in the moduli is much smaller in film region 2, and a discontinuity in characteristic time for the film formation is observed between both film regions. Results from the kinetic study can be modeled to estimate the thermodynamic transition temperatures, and obtain the thermodynamic 2D phase diagram. A procedure to do this has been illustrated for a 20 wt% solution. Further study of different models at multiple concentrations is necessary to obtain a good estimate of the thermodynamic 2D phase diagram.

Chapter 7

EXAMINING THE PROPERTIES OF THE FILM

The existence of two distinct phases at the interface has been shown in chapter 4, 5 and 6: Film region 1 and film region 2. In this chapter the properties of both phases are further investigated. Strain amplitude and frequency sweeps are examined to characterize the microstructure of the film in both regions.

7.1 Strain Amplitude Sweep

In a strain amplitude sweep, the moduli are measured varying the strain amplitude γ_0. For low strains or equivalently low stresses, the microstructure of the material is preserved and not influenced by the stresses applied. In this region the moduli obtained from oscillatory shear measurements characterize the material without affecting the microstructure. This region is the linear regime. This is the region where the stress is proportional to the strain, and the loss angle is independent of the strain amplitude [9]. This is equivalent to the region where the moduli are independent of the strain amplitude. At higher strains the stress affects the microstructure, and yielding occurs. The strain at which yielding occurs can be used to determine the yield stress of the material.

A strain amplitude sweep of 20 wt% L64 in D_2O at 43 ºC and 55 ºC on a cone and plate geometry is shown in figure 25 and 26 respectively.

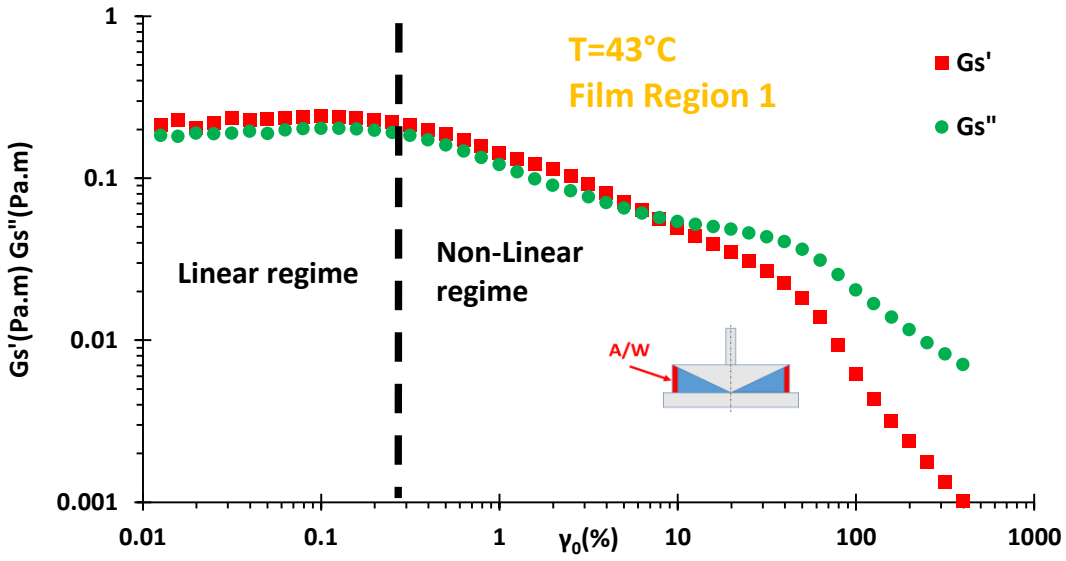

Figure 25: Strain amplitude sweep on a cone and plate geometry (d_c=50mm, φ=0.0195 rad) for 20wt% L64 in D_2O at T=43ºC, and ω=1.36rad/s.

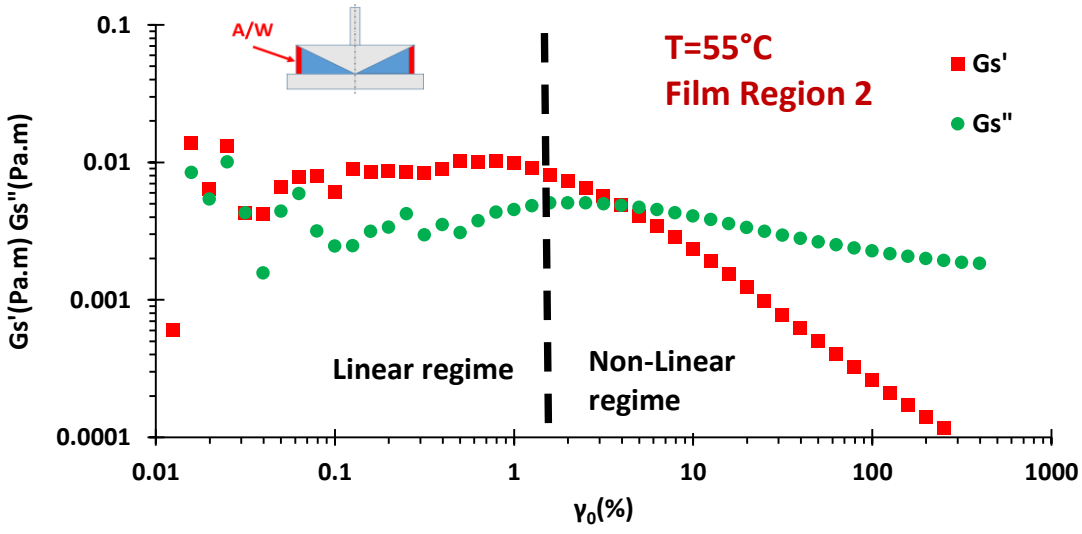

Figure 26: Strain amplitude sweep on a cone and plate geometry (d_c=40mm, φ=0.0195 rad) for 20wt% L64 in D_2O at T=55ºC, and ω=1.36rad/s.

In film region 1, the linear regime is valid for $\gamma_0 < 0.2\%$. For film region 2 the linear regime is valid for $\gamma_0 < 1.5\%$. For higher strain amplitudes yielding occurs and the microstructure of the film is affected. This yielding is characterized by a drop in both moduli, where the storage modulus drops faster. The storage modulus drops below the loss modulus, meaning that the elasticity decreases. The complex modulus decreases, meaning that the rigidity of the material decreases. In literature a high strain has been used in the nonlinear regime [7]. This is why in literature and equivalently in figure 6 the apparent loss modulus is higher than the apparent storage modulus for all temperatures and as a result the elasticity of the film is underestimated. To determine the properties of the film and its microstructure it is important to work in the linear regime where the microstructure is not affected by the high stresses.

7.2 Frequency Sweep

By varying the frequency the structural response at different time scales can be evaluated. Figure 27 and 28 show the frequency sweeps for a temperature in film region 1 and 2 respectively.

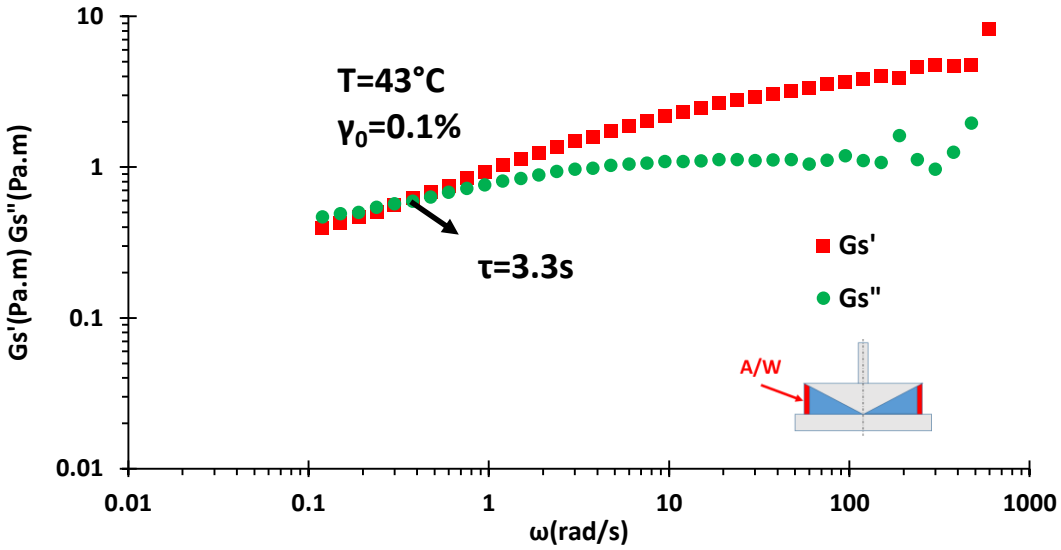

Figure 27: Frequency sweep on a cone and plate geometry (d_c=50mm, φ=0.0195 rad) for 20wt% L64 in D_2O at T=40°C, and γ_0=0.1%.

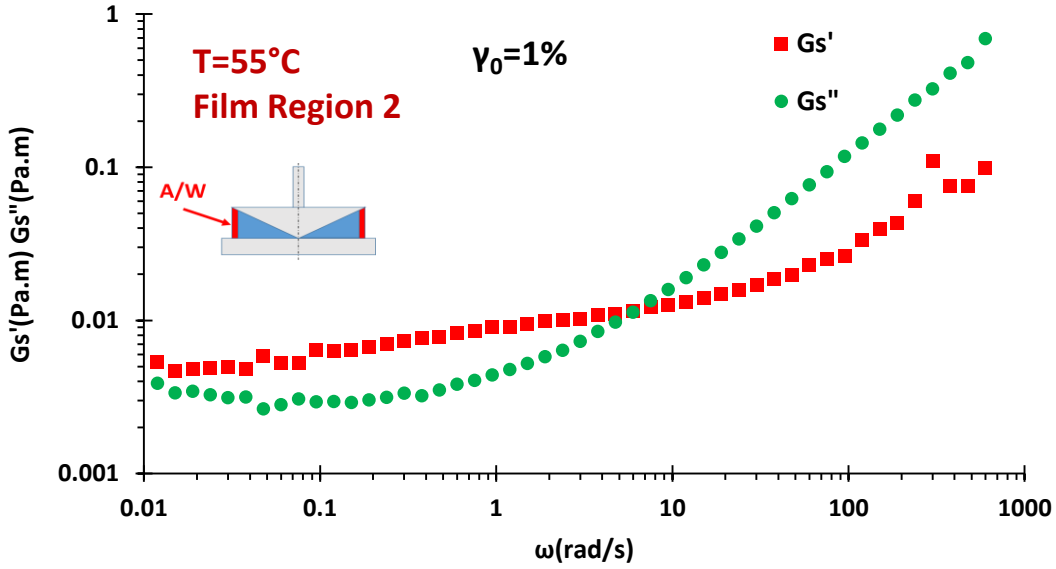

Figure 28: Frequency sweep on a Cone and Plate geometry (d_c=50mm, φ=0.0195 rad) for 20wt% L64 in D_2O at T=55°C, and γ_0=1%.

The observed frequency dependence of the moduli is typical for a viscoelastic fluid for both regions of the film: At low frequency the response is more viscous (G″>G′) and at high frequency the response is more elastic (G″<G′) [9]. This suggests that the film is viscoelastic. For a viscoelastic fluid following the Maxwell fluid the frequency where the loss and storage moduli cross over is related to the relaxation time (τ): $\tau = 1/\omega$ [9]. At 43 ºC in film region 1 the relaxation time of the system is 3.3s.

At first sight the results of the frequency and strain sweeps at 43 °C in figure 25 and 27 seem to be inconsistent. The corresponding values of the surface moduli are lower in the strain sweep than in the frequency sweep. This is a consequence of the fact that the surface moduli continue to grow in time even after hours, and thus have not reached steady state yet during the strain and amplitude sweeps. In the frequency sweep of figure 27 the film has had more time to grow than in the strain sweep of figure 25, leading to this apparent inconsistency. Other measurements at different equilibration times have shown that the strain amplitudes show the same trend, with the same linear regime independent of the equilibration time used.

In film region 2 the frequency sweep also shows the behavior of a viscoelastic fluid according to the Maxwell model. The first crossover is expected to happen at lower frequencies, and is not measured. This corresponds to a lower characteristic frequency, or higher timescales compared to film region 1. In this case the crossover corresponds to a relaxation time longer than 100s. At higher frequencies, the loss modulus crosses over the storage modulus, as is expected for the Maxwell model [9].

7.3 Conclusion

The strain amplitude and frequency sweeps of the film show a viscoelastic behavior that differs in both film regions. In film region 1 the linear regime is valid for $\gamma_0 < 0.2\%$ and for film region 2 the linear regime is valid for $\gamma_0 < 1.5\%$. The relaxation time according to the Maxwell model is 3.3 s in film region 1, and it is longer than 100 s in film region 2.

Chapter 8

THE EFFECT OF INTERFACIAL FILMS ON BULK RHEOLOGY MEASUREMENTS

The formation of a film at the interface can greatly affect bulk rheology measurements and lead to misinterpretation of data. The bulk rheology measurements assume that the interfacial contributions are negligible. The surface viscosity of a film is usually much higher than the bulk viscosity and as a consequence very thin films can already have a significant effect on bulk rheology measurements. Aqueous solutions of pluronic L64 are a good example to show how the formation of a film at the interface can affect rheology measurements. The effect on oscillatory shear measurements have already been widely discussed in chapter 4 and 5, but are shortly reviewed in this chapter. The effect on steady shear rheology measurements are examined in detail, and a procedure to measure and take into account the interfacial effect is discussed.

8.1 Oscillatory Shear Rheology Measurements

As shown in chapter 4 and 5, the formation of a film at the air-water interface in L64 solutions in D_2O greatly affect the oscillatory shear measurements. The apparent moduli measured by the instruments are in fact due to both bulk and surface contributions, while the theory assumes the surface contributions is negligible. In this case the interfacial contribution completely dominates the response in cone and plate geometries and even in couette geometries when they are set to be sensitive to the air-liquid interface. As a result measurements of the apparent moduli can lead to wrong interpretation of data. In this case a percolation phenomenon was attributed to the sudden increase in the apparent moduli, while this increase was actually due to the

interfacial film contribution. In other cases the contribution might be smaller but still significant. This can lead to overestimations of the bulk moduli, and can change the measured elasticity of the sample by affecting the loss angle δ.

When surface active components are present it is important to consider the effect of the interfacial viscosity. Other systems have shown the same interfacial effect. Bovine Serum Albumin (BSA) solutions is an example a protein solution where the interfacial contribution also affects the bulk rheology measurements [1].

8.2 Steady Shear Rheology Measurements

In steady shear rheology measurements the sample is steadily deformed at a certain shear rate. The viscosity is often measured at varying shear rates to characterize the behavior of materials under stresses. The formation of a film at the interface can also affect steady shear measurements. This is illustrated for a 20 wt% solution of L64 in D_2O, where steady shear measurements are compared in the interface sensitive cone and plate geometry and the interface insensitive couette geometry. The results are shown for different temperatures in the different film regions in figure 29.

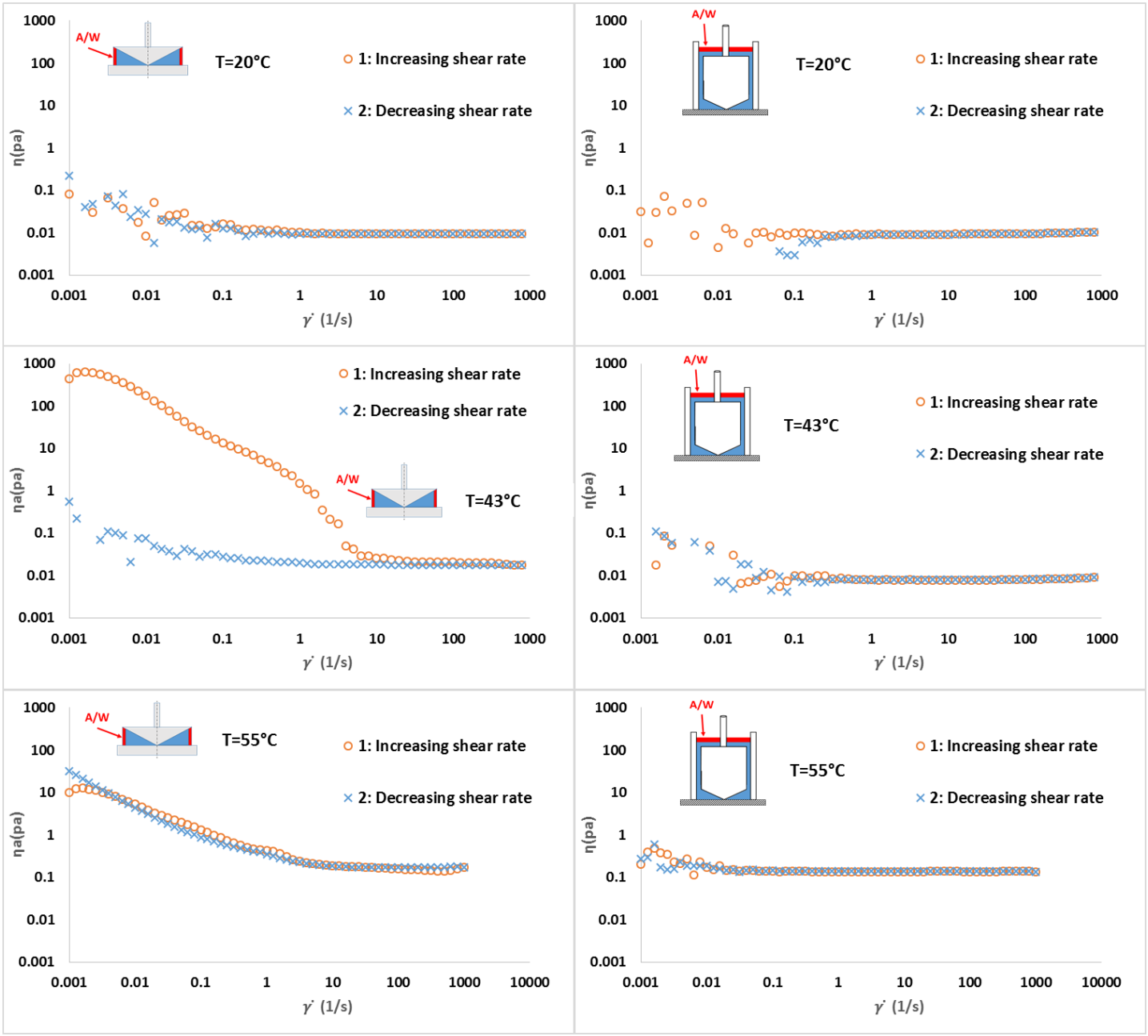

Figure 29: Steady shear rheology measurements of 20 wt% L64 in D_2O at different temperatures on a cone and plate geometry with d_c=50mm and φ=0.0195rad (left) and on a DIN couette geometry with D_b=27.7mm, D_c=30mm and L_b=41.6mm (right). The equilibration time is 1 hour at 20 °C, 2 hours at 43°C and 40 mins at 55 °C. 10 points per decade are measured, and each point is averaged for 15 seconds with 15 seconds equilibration time.

At 20 °C there is no significant difference between the C/P and the Couette geometry results. In this state no interfacial contribution is detected in the C/P geometry and thus the steady shear rheology measurements are not affected by interfacial effects.

At 43 °C the results in the C/P and the Couette geometry are completely different. At this temperature and concentration the interface is in film region 2, as can be seen in the apparent 2D phase diagram in figure 16. The measurements in the C/P geometry show an apparent yield stress, and a shear thinning behavior while the Couette geometry results show Newtonian behavior. This is due to the interfacial contribution. The addition of the interfacial shear thinning behavior onto the bulk Newtonian behavior gives rise to an apparent shear thinning behavior measured in the C/P geometry. This leads to wrong conclusions whenever the interfacial contribution is not accounted for.

At 55 °C in film region 2, the same apparent shear thinning behavior is observed for the C/P geometry.

In both film region 1 and 2 steady shear measurements in the C/P geometry show an apparent but different shear thinning behavior. In film region 1 the zero shear viscosity is an order of magnitude higher than in film region 2. This is consistent with the higher apparent moduli measured in the oscillatory shear measurements. The reversibility of the apparent shear thinning behavior is different in each case. In film region 1 hysteresis in the steady shear measurements is observed. The viscosity does not follow the same path when going back down in shear rate. In film region 2 the results are almost perfectly reversible. This is another indication that the structure of both film regions are completely different. For film region 1 the decreasing shear rate

curve is almost the same as for the couette geometry. This means that the film in region 1 is completely broken down by the high shear rates and, in the time given, is barely able to reform. For film region 2, the film shear thins, but is not broken down by the high shear rates.

8.3 Process to Detect the Interfacial Contribution

It is important to consider the interfacial contribution, especially in systems with surface active components.

To avoid the interfacial contribution, geometries that are insensitive to the interface can be used. In this case the couette geometry can be used for this purpose. The disadvantage is that these geometries usually require more sample volume. The surface viscosity and moduli can also directly be measured with geometries that probe the interface, like for example the Double Wall Ring (DWR) geometry (© TA Instruments). This allows to determine whether or not the interfacial contribution is negligible in a certain bulk geometry. Another way to determine if an interfacial contribution is present is to use multiple geometries. The results of rheology measurements should be the same independent of the used geometry. If however the contribution from the interface is important, the results will differ for different geometries as the interfacial contribution is different in each case.

8.4 Conclusion

Rheological measurements can be greatly affected by the presence of a film at the interface. This can lead to misinterpretation of data when the interfacial contribution is neglected. In this system the interfacial contribution leads to an

apparent shear thinning behavior, and to apparent moduli that are completely dominated by the surface moduli.

The apparent shear thinning behavior is different in both film regions. Film region 1 shows an important hysteresis, while the results in film region 2 are almost completely reversible. The high shear rates completely break down the film in region 1 but barely affect it in region 2.

It is important to consider the interfacial contribution, especially in systems with surface active components. By varying the geometries or by measuring the interfacial rheology directly the interfacial contribution can be measured and taken into account if necessary.

Chapter 9

CONCLUSION AND FUTURE WORK

A viscoelastic film is formed at the air-water interface in aqueous solutions of pluronic L64. A direct interfacial measurement of the apparent surface tension and rheology measurements on different geometries provide direct evidence to the formation of this film at the air-water interface. SANS measurements and rheology measurements on different geometries show that the apparent increase of the moduli in solutions of pluronic L64 in D_2O is not an indication of a percolation phenomenon, but is due to the formation of this film at the air-water interface. The bulk rheology measurements are affected by the interface in such a way that the Boussinesq number for the cone and plate geometry is high enough to dominate the results and can be used to determine the surface properties of the film. The 2D apparent phase diagram is constructed in the concentration range of 5 to 25 wt%. The formation of the film is a very slow process, and for this reason it gives rise to an 'apparent' phase diagram, defined at a temperature rate of 0.1 °C/min. The kinetics of the formation of the film are investigated to quantify the time necessary for the film to form and the rate at which the response of the film grows. The formation of the film shows properties similar to a nucleation process. The results of the kinetic study can be used to predict the thermodynamic 2D phase diagram. Two distinct phases are observed at the air-water interface: film region 1 and film region 2. The surface moduli are 1 order of magnitude smaller in region 2. The strain amplitude and frequency sweeps of the film show that both regions have different properties with viscoelastic characteristics. The relaxation time according to the Maxwell model is 3.3 s in film region 1, and it is longer than 100 s in film region 2. The apparent shear thinning behavior is different in

both film regions. The high shear rates completely break down the film in region 1 but barely affect it in region 2.

Rheological measurements can be greatly affected by the presence of a film at the interface. This can lead to misinterpretation of data when the interfacial contribution is neglected. In this system the interfacial contribution leads to an apparent shear thinning behavior. For example it has also lead to the idea of a percolation phenomenon. It is important to consider the interfacial contribution, especially in systems with surface active components. By varying the geometries or by measuring the interfacial rheology directly the interfacial contribution can be measured and properly taken into account if necessary.

This thesis has established a first study of the film formed in aqueous solutions of pluronic L64. Future work is necessary to better understand the mechanism of formation, and the properties of the different film phases. More direct film characterization methods such as ellipsometry, spectral X-ray or neutron reflectometry can be used to determine the dynamics, the structure and the thickness of the film.

REFERENCES

[1] V. Sharma, A. Jaishankar, Y. Wang and G. McKinley, "Rheology of globular proteins: apparent yield stress, high shear rate viscosity," *Soft Matter,* no. 7, pp. 5150-5160, 2011.

[2] S. Campioni, G. Carret, S. Jordens, L. Nicoud, R. Mezzenga and R. Riek, "The Presence of an Air−Water Interface Affects Formation and Elongation of α-Synuclein Fibrils," *Journal of the American Chemical Society,* vol. 136, no. 7, pp. 2866-2875, 2014.

[3] J. Hao, Self-Assembled Structures: Properties and applications in solution and on surfaces, Taylor & Francis Group, 2011.

[4] P. Alexandridis and T. Hatton, *Colloïds and Surface A,* vol. 96, no. 1-2, pp. 1-46, 1995.

[5] R. Liu, Water-Insoluble Drug Formulation, Taylor & Francis Group, 2008.

[6] E. Batrakova and A. Kabanov, "Pluronic block copolymers: Evolution of drug delivery concept from inert nanocarriers to biological response modifiers," *Journal of Controlled Release,* vol. 130, pp. 98-106, 2008.

[7] L. Lobry, N. Micali, F. Mallamace, C. Liao and S. Chen, "Interaction and percolation in the L64 triblock copolmer micellar system," *Phys Rev E,* vol. 60, no. 6, pp. 7076-87, 1999.

[8] H. A. Barnes, J. F. Hutton and K. Walters, An Introduction to Rheology, Amsterdam: Elsevier, 1989.

[9] J. Mewis and N. Wagner, Colloidal Suspension Rheology, New York: Cambridge University Press, 2012.

[10] R. Pynn, Neutron Scattering: A primer, LANSCE, 1990.

[11] B. Hammouda, Probing Nanoscale Structures - The SANS Toolbox, Gaithersburg, Maryland, 2010.

[12] P. Ghosh, Colloid and Interface Science, New Delhi: PHI Learning Private Limited, 2009.

[13] S. R. Kline, "Reduction and Analysis of SANS and USANS Data using Igor Pro," *J Appl. Cryst. ,* vol. 39, no. 6, p. 895, 2006.

[14] D. Edwards, H. Brenner and D. Wasan, Interfacial Transport Processes and Rheology, Boston: Butterworth-Heinemann, 1991.